On a hierarchical estimator driven by a stabilized method for the reactive incompressible Navier–Stokes equations

Rodolfo Araya [1], Abner H. Poza

Departamento de Ingeniería Matemática
Universidad de Concepción
Casilla 160-C, Concepción, Chile

and

Frédéric Valentin

Departamento de Matemática Aplicada
Laboratório Nacional de Computação Científica
Av. Getúlio Vargas, 333, 25651-075 Petrópolis - RJ, Brazil

Abstract

This work concerns with compounding two complementary strategies to accurately solve the reactive incompressible Navier-Stokes model, namely, a stabilized method and a mesh refinement approach relied on an error estimator. We adopt equal order interpolation spaces to approach both the velocity and the pressure, and the stability is recovered from a new unusual stabilized finite element method. The method is designed to deal with reactive and advective dominate flows through a threefold asymptotic behavior of the stabilization parameter. Mesh adaptivity driven by a new hierarchical error estimator and built on the unusual method is the second ingredient. The estimator circumvents the saturation assumption by using an enhanced space strategy and shows to be equivalent to the error. Several numerical tests validate the combined methodology.

Email addresses: raraya@ing-mat.udec.cl (Rodolfo Araya), abner@ing-mat.udec.cl (Abner H. Poza), valentin@lncc.br (Frédéric Valentin).

[1] Corresponding author. Tel.: +56 41 2204103; Fax: +56 41 2522055.

1 Introduction

Detailed representation of flow structure passes necessarily by mesh refinements which in turn demand prior knowledge on approximation errors. That is the role played by a posteriori error estimators which require accuracy, in the sense of being equivalent to the error, and affordability from computational viewpoint. Those needed features are, nevertheless, insufficient as long as complex flows driven by the reactive incompressible Navier-Stokes model are concerned. As a matter of fact, reliable error estimators must involve stable and accurate finite element methods whenever we want appropriate adapted meshes. Hence, this work is a twofold contribution in which a new unusual stabilized finite element method is combined with a new a posteriori hierarchical error estimator to solve reactive and advective dominate flows.

Unusual stabilized finite element methods are particularly desirable when it comes to approach reactive dominate problems as generalized Stokes models [3,8] or reactive-advective-diffusive problems [19,26,30,31]. Roughly, those methods are composed by the standard Galerkin terms subtracted (being this the reason of its denomination) by a L^2-inner product involving the residual of strong equation balanced by the so-called stabilization parameter. Recently, their effective forms have been recovered by enhancing polynomial spaces with multi-scale functions which correspond to element-wise solution of original operator with the right hand side defined in terms of residuals on elements and edges. See [3,7,21,22] for further details.

The present work extends the unusual method introduced and analyzed in [26] to the reactive incompressible Navier-Stokes equations adopting equal order pair of interpolation spaces. What emerges is a finite element method ready to deal with the matter of the compatibility between the pressure and velocity spaces (in the sense of inf–sup condition) while it handles exponential and parabolic boundary layers accurately [38]. In addition, the method will take advantage of adapted meshes to overcome local over and undershooting numerical solutions without asking for shock capturing methodologies [2,32]. Interested readers may find related works in [14,16].

Involve a posteriori error estimators to account for the quality of discrete solutions of the Navier–Stokes equations has been addressed through residual-based [12,34], goal oriented [10,11] or local problems error estimates [33,36]. Readers can find further references in [1,6,42]. In this work we adopt the hierarchical approach first developed in [4] for the generalized Stokes equations. Mesh adaptativity by hierarchical approach appears as an elegant technique to construct a posteriori error estimators without demanding the well-know saturation assumption [1,5]. The idea is to adopt an auxiliary linear problem at the local level for which the solution is shown to be equivalent to the error

but easier to be calculated. It is, actually, obtained by projecting the finite element error onto the finite element space enhanced with bubble functions.

The outline of this manuscript is as follows: Some standard notations and definitions finalize the current section. In Section 2 we introduce the reactive Navier-Stokes equations and we state some classical results. The unusual method is presented in Section 3. Section 4 concerns with the derivation and analysis of the hierarchical estimator. The paper ends with several numerical tests in Section 5.

1.1 Notations and Definitions

This section introduces definitions and notations used throughout. In what follows, $\Omega \subseteq \mathbb{R}^2$ denotes an open bounded set with polygonal boundary Γ, and $\boldsymbol{x} = (x_1, x_2)$ is a typical point in Ω. As usual, $L^2(\Omega)$ is the space of square integrable functions over Ω, $L^2_0(\Omega)$ represents functions belonging to $L^2(\Omega)$ with zero average in Ω, and $H^m(\Omega)$ is composed by functions whose m first derivatives belong to $L^2(\Omega)$. We use the convention $H^0(\Omega) = L^2(\Omega)$. Moreover, $(\cdot\,,\cdot)_D$ stands for the inner product in $L^2(D)$ (or in $L^2(D)^2$, when necessary), and $\|\cdot\|_{s,D}$ ($|\cdot|_{s,D}$) the norm (seminorm) in $H^m(D)$ (or $H^m(D)^2$, if necessary).

From now on, we denote by $\{\mathcal{T}_h\}_{h>0}$ a regular family of triangulations of Ω composed by elements T and by $\mathcal{E}_h$ the set of all edges of $\mathcal{T}_h$ with the usual splitting $\mathcal{E}_h = \mathcal{E}_\Omega \cup \mathcal{E}_\Gamma$, where $\mathcal{E}_\Omega$ stands for the edges lying in the interior of Ω. As usual h_T means the diameter of T, $h = \max_{T\in\mathcal{T}_h} h_T$ and $h_F := |F|, \quad F \in \mathcal{E}_h$. Also, for $T \in \mathcal{T}_h$, we denote by $\mathcal{N}(T)$ the set of nodes of T and by $\mathcal{E}(T)$ the set of edges of T. Given $T \in \mathcal{T}_h$ and $F \in \mathcal{E}_h$ we define the following neighborhoods:

$$\omega_T := \bigcup_{\mathcal{E}(T)\cap\mathcal{E}(T')\neq\emptyset} T' \quad , \quad \widetilde{\omega}_T := \bigcup_{\mathcal{N}(T)\cap\mathcal{N}(T')\neq\emptyset} T',$$
$$\omega_F := \bigcup_{F\in\mathcal{E}(T')} T' \quad , \quad \widetilde{\omega}_F := \bigcup_{\mathcal{N}(F)\cap\mathcal{N}(T')\neq\emptyset} T'.$$

Furthermore, for each $F = \partial T \cap \partial T^{'} \in \mathcal{E}_h$ and for a function q, one denotes $[\![q]\!]_F$ its jump, defined by:

$$[\![q]\!]_F(\boldsymbol{x}) := \lim_{\delta\to 0^+} q(\boldsymbol{x} + \delta\boldsymbol{n}_F) - \lim_{\delta\to 0^-} q(\boldsymbol{x} - \delta\boldsymbol{n}_F)\,,$$

where $\boldsymbol{n}_F$ stands for the outward normal vector at the edge F with respect to T. Note that $[\![q]\!]_F = 0$ if $F \subseteq \Gamma$.

Finally, the following convention is adopted

$$a \preceq b \Longleftrightarrow a \leq K\, b,$$
$$a \simeq b \Longleftrightarrow a \preceq b \text{ and } b \preceq a,$$

where the positive constant K is independent of h, σ and ν.

2 Model problem

The reactive stationary incompressible Navier-Stokes problem consists of finding the velocity vector field $\boldsymbol{u}$ and the pressure scalar field p such that

$$(P)\quad \begin{cases} -\nu\,\Delta \boldsymbol{u} + (\nabla \boldsymbol{u})\boldsymbol{u} + \sigma\,\boldsymbol{u} + \nabla p = \boldsymbol{f} & \text{in} \quad \Omega, \\ \text{div}\ \boldsymbol{u} = 0 & \text{in} \quad \Omega, \\ \boldsymbol{u} = \boldsymbol{0} & \text{on} \quad \Gamma, \end{cases}$$

where the reaction and the viscosity coefficient σ and ν, respectively, are assumed positive constant in Ω. Here, $\boldsymbol{f}$ is a regular given function representing the source term.

Let us set $\boldsymbol{H} := H_0^1(\Omega)^2$ and $Q := L_0^2(\Omega)$ and propose the following weak formulation for the problem (P): *Find* $(\boldsymbol{u}, p) \in \boldsymbol{H} \times Q$ *such that*

$$a(\boldsymbol{u}, \boldsymbol{v}) + b(\boldsymbol{u}, q) + b(\boldsymbol{v}, p) + c(\boldsymbol{u}; \boldsymbol{u}, \boldsymbol{v}) = (\boldsymbol{f}, \boldsymbol{v})_\Omega \qquad \forall\, (\boldsymbol{v}, q) \in \boldsymbol{H} \times Q, \quad (2.1)$$

where the bilinear forms $a(\cdot,\cdot)$ and $b(\cdot,\cdot)$, and the trilinear form $c(\cdot,\cdot,\cdot)$ are given by

$$a(\boldsymbol{u}, \boldsymbol{v}) := \nu(\nabla \boldsymbol{u}, \nabla \boldsymbol{v})_\Omega + \sigma(\boldsymbol{u}, \boldsymbol{v})_\Omega\,, \quad (2.2)$$
$$b(\boldsymbol{v}, q) := -\,(q, \text{div}\, \boldsymbol{v})_\Omega\,, \quad (2.3)$$
$$c(\boldsymbol{u}; \boldsymbol{v}, \boldsymbol{w}) := ((\nabla \boldsymbol{v})\boldsymbol{u}, \boldsymbol{w})_\Omega\,. \quad (2.4)$$

Furthermore, we introduce the symmetric bilinear form $d : Q \times Q \to \mathbb{R}$ by

$$d(p, q) := \frac{1}{\nu}\,(p, q)_\Omega\,,$$

which induces the norms

$$\|\boldsymbol{v}\|_a := a(\boldsymbol{v}, \boldsymbol{v})^{1/2} \qquad \forall \boldsymbol{v} \in \boldsymbol{H}, \quad (2.5)$$
$$\|q\|_d := d(q, q)^{1/2} \qquad \forall q \in Q\,, \quad (2.6)$$

as well as the norm on the product space $\boldsymbol{H} \times Q$

$$\|(\boldsymbol{v}, q)\| := \left\{ \|\boldsymbol{v}\|_a^2 + \|q\|_d^2 \right\}^{1/2} \qquad \forall (\boldsymbol{v}, q) \in \boldsymbol{H} \times Q \,.$$

The next result states some inequalities which will be used in the sequel.

Lemma 1 *Let $a(\cdot,\cdot)$ and $b(\cdot,\cdot)$ be the bilinear forms given by (2.2) and (2.3), respectively, and let $c(\cdot,\cdot,\cdot)$ the trilinear form given by (2.4). Then*

$$|a(\boldsymbol{v}, \boldsymbol{w})| \leq \|\boldsymbol{v}\|_a \|\boldsymbol{w}\|_a \qquad \forall\, \boldsymbol{v}, \boldsymbol{w} \in \boldsymbol{H} \,, \tag{2.7}$$

$$|b(\boldsymbol{v}, q)| \leq \sqrt{2}\, \|\boldsymbol{v}\|_a \|q\|_d \qquad \forall (\boldsymbol{v}, q) \in \boldsymbol{H} \times Q \,, \tag{2.8}$$

$$\sup_{\boldsymbol{v} \in \boldsymbol{H}} \frac{b(\boldsymbol{v}, q)}{\|\boldsymbol{v}\|_a} \geq \alpha_b \sqrt{\frac{\nu}{\sigma + \nu}}\, \|q\|_d \qquad \forall q \in Q \,, \tag{2.9}$$

$$c(\boldsymbol{w}; \boldsymbol{u}, \boldsymbol{v}) \leq \beta\, |\boldsymbol{w}|_{1,\Omega} |\boldsymbol{u}|_{1,\Omega} |\boldsymbol{v}|_{1,\Omega} \qquad \forall\, \boldsymbol{v}, \boldsymbol{w} \in \boldsymbol{H} \,, \tag{2.10}$$

where α_b and β are positive constants depending only on Ω. Moreover, for all $\boldsymbol{u}, \boldsymbol{v}, \boldsymbol{w} \in \boldsymbol{H}$ such that $\operatorname{div} \boldsymbol{w} = 0$, *and $\boldsymbol{w} \cdot \boldsymbol{n} = 0$, there holds*

$$c(\boldsymbol{w}; \boldsymbol{u}, \boldsymbol{v}) = -c(\boldsymbol{w}; \boldsymbol{v}, \boldsymbol{u}), \tag{2.11}$$

$$c(\boldsymbol{w}; \boldsymbol{v}, \boldsymbol{v}) = 0. \tag{2.12}$$

PROOF. The proof follows from the norm definitions (2.5)-(2.6) and from classical results in [28]. □

The next classical result is included for sake of completeness and addresses the well-posedness of (2.1).

Theorem 2 *Assume that ν and $\boldsymbol{f} \in L^2(\Omega)^2$ satisfy the following condition:*

$$|(\boldsymbol{f}, \boldsymbol{v})_\Omega| \leq \gamma \frac{\nu^2}{\beta}\, |\boldsymbol{v}|_{1,\Omega} \qquad \forall \boldsymbol{v} \in \boldsymbol{H} \,,$$

for some fixed number $\gamma \in [0, 1)$. Then, there exits an unique solution $(\boldsymbol{u}, p) \in \boldsymbol{H} \times Q$ of (2.1) and it holds

$$|\boldsymbol{u}|_{1,\Omega} \leq \gamma\, \frac{\nu}{\beta}. \tag{2.13}$$

PROOF. See Theorem 2.4, Chapter IV in [28]. □

3 The Unusual Stabilized Method

This section proposes a stabilized finite element method to solve (2.1) and we select the approximate subspaces $\boldsymbol{H}_h \subset \boldsymbol{H}$ and $Q_h \subset Q$ as follow

$$\begin{aligned}\boldsymbol{H}_h &:= \{\boldsymbol{v}_h \in C(\overline{\Omega})^2 : \boldsymbol{v}_h|_T \in \mathbb{P}_k(T)^2, \forall T \in \mathcal{T}_h\} \cap \boldsymbol{H},\\ Q_h &:= \{q_h \in C(\overline{\Omega}) : q_h|_T \in \mathbb{P}_l(T), \forall T \in \mathcal{T}_h\} \cap Q\,,\end{aligned}$$

where $k, l \in \mathbb{N}^+$.

Remark 3 *The LBB condition prevents equal order interpolation spaces ($k = l$) for the velocity and the pressure to be used along with the Galerkin method (see [13]). The symptoms of this likely practitioner choice are numerical solutions plagued by spurious oscillations. Unfortunately that is not the only potencial source of instabilities. Indeed, dominate reaction and/or advection flows are also badly approached by the classical Galerkin as soon as the underlying flows include sharp boundary layers.* □

Next, we tackle both source of instabilities by proposing the following unusual stabilized finite element method: *Find* $(\boldsymbol{u}_h, p_h) \in \boldsymbol{H}_h \times Q_h$ *such that:*

$$\boldsymbol{B}((\boldsymbol{u}_h, p_h), (\boldsymbol{v}_h, q_h)) \;=\; \boldsymbol{F}(\boldsymbol{v}_h, q_h) \qquad \forall (\boldsymbol{v}_h, q_h) \in \boldsymbol{H}_h \times Q_h\,, \tag{3.14}$$

with

$$\begin{aligned}&\boldsymbol{B}((\boldsymbol{u}_h, p_h), (\boldsymbol{v}_h, q_h)) := a(\boldsymbol{u}_h, \boldsymbol{v}_h) + b(\boldsymbol{u}_h, q_h) + b(\boldsymbol{v}_h, p_h) + c(\boldsymbol{u}_h; \boldsymbol{u}_h, \boldsymbol{v}_h)\\ &- \sum_{T\in\mathcal{T}_h} \Big((\nabla \boldsymbol{u}_h)\boldsymbol{u}_h - \nu\,\Delta \boldsymbol{u}_h + \sigma \boldsymbol{u}_h + \nabla p_h, \tau_T\,[-(\nabla \boldsymbol{v}_h)\boldsymbol{u}_h - \nu\,\Delta \boldsymbol{v}_h + \sigma \boldsymbol{v}_h + \nabla q_h] \Big)_T\\ &+ \sum_{T\in\mathcal{T}_h} (\operatorname{div} \boldsymbol{u}_h, \delta_T \operatorname{div} \boldsymbol{v}_h)_T,\end{aligned} \tag{3.15}$$

and

$$\boldsymbol{F}(\boldsymbol{v}_h, q_h) := (\boldsymbol{f}, \boldsymbol{v}_h)_\Omega - \sum_{T\in\mathcal{T}_h} \Big(\boldsymbol{f}, \tau_T\,[-(\nabla \boldsymbol{v}_h)\boldsymbol{u}_h - \nu\,\Delta \boldsymbol{v}_h + \sigma \boldsymbol{v}_h + \nabla q_h] \Big)_T.$$

The stability and accuracy of the method relies on the definition of parameters δ_T and τ_T. Here, those piecewise constant functions are defined by

$$\delta_T := \|\boldsymbol{u}_h\|_{\infty,T}\, h_T\, \min\{1, Re_T^2\}\,, \quad \tau_T := \frac{h_T^2}{\sigma\, h_T^2\, \xi(Re_T^1) + \dfrac{2\,\nu}{m_k}\, \xi(Re_T^2)}\,, \tag{3.16}$$

with $\xi(x) := \max\{1, x\}$ and

$$Re_T^1 := \frac{2\,\nu}{\sigma\, h_T^2\, m_k}, \quad Re_T^2 := \frac{\|\boldsymbol{u}_h(x)\|_{\infty,T}\, h_T\, m_k}{4\,\nu}, \quad m_k := \min\left\{\frac{1}{3}, 2\, C_I^k\right\}.$$

The positive constant C_I^k is related to the inverse inequality

$$C_I^k\, h_T^2\, \|\Delta \boldsymbol{v}_h\|_{0,T}^2 \leq \|\nabla \boldsymbol{v}_h\|_{0,T}^2 \qquad \forall \boldsymbol{v}_h \in \boldsymbol{H}_h\,. \tag{3.17}$$

Lemma 4 *For all $T \in \mathcal{T}_h$, the parameters δ_T and τ_T given by (3.16) satisfy:*

$$\tau_T\, \|\boldsymbol{u}_h\|_{\infty,T} \leq \frac{1}{2}\, h_T, \tag{3.18}$$

$$\tau_T\, \nu \leq \frac{1}{6}\, h_T^2, \tag{3.19}$$

$$\tau_T\, \sigma \leq \min\{h_T\, \sigma^{1/2}\, \nu^{-1/2}, 1\}, \tag{3.20}$$

$$\delta_T \leq \|\boldsymbol{u}_h\|_{\infty,T} h_T. \tag{3.21}$$

PROOF. The result is a straight consequence of the definition of δ_T and τ_T. □

Remark 5 *The unusual method* (3.14) *extends the one primarily proposed for the linear advective-diffusive model in [26]. Likewise, it coincides with the Galerkin-Least-Square method [18] when σ vanishes as the stabilization parameter in [18] can be rewritten in a equivalent way as*

$$\tau_T = \frac{h_T^2\, m_k}{2\,\nu\, \xi(Re_T^2)}\,.$$

□

Remark 6 *As far as the vanishing advection case is concerned, we recover the method proposed in [8,3] by setting δ_T equals to zero and assuming linear interpolation for both velocity and pressure spaces. Those underlined methods are obtained by enriching the linear finite element spaces with multi-scale functions which are computed from local elliptic boundary value problem for the velocity. On the other hand, enhancing the standard space for the pressure with bubbles functions adds a divergence least-square term in the Galerkin method analogous to the one used in* (3.14) *(see [23]) . Consequently, enriching space approach stems as a general framework to build stable methods and to set up the parameters τ_T and γ.* □

Remark 7 *In order to handle discontinuous interpolation for the pressure in* (3.14)*, extra stability should be included and relied on inter-element boundary jump pressure terms (see [25,40] for further discussion). As for higher order continuous interpolation spaces, the method demands computing the inverse*

inequality constant exactly. This may be achieved in an elegant way by computing the smaller generalized eigenvalue of the problem associated to (3.17) *in each element (see [20]).* □

Remark 8 *It may be worth taking into account element-wise directional information of velocity field* $\boldsymbol{u}$ *in order to compute the characteristic element length* h_T *for advective dominate problems. This has been numericaly highlighted in [26] after having been formally derived in [24] within the Residual-Free Bubble (RFB) framework.* □

4 An a posteriori error estimate

This section establishes a hierarchical *a posteriori* error estimator by extending the ideas of [4] to the reactive Navier-Stokes equation (P).

4.1 Preliminary results

By $I_h : \boldsymbol{H} \longrightarrow \boldsymbol{H}_h$ we denote the Clément interpolation operator (cf. [15,17]). For all $T \in \mathcal{T}_h$ and all $F \in \mathcal{E}(T)$ this operator satisfies

$$|\boldsymbol{v} - I_h\boldsymbol{v}|_{m,T} \preceq h_T^{n-m}\,|\boldsymbol{v}|_{n,\widetilde{\omega}_T}\,, \tag{4.1}$$

$$\|\boldsymbol{v} - I_h\boldsymbol{v}\|_{0,F} \preceq h_F^{n-\frac{1}{2}}\,|\boldsymbol{v}|_{n,\widetilde{\omega}_F}\,, \tag{4.2}$$

for all $\boldsymbol{v} \in H^n(\Omega)^2$, and all $0 \leq m \leq 1$, $1 \leq n \leq k+1$. We need in the sequel some mesh–dependent constants defined as follows:

$$\theta_T := \begin{cases} \nu^{-1/2}\,h_T & ,\sigma = 0\,, \\ \sigma^{-1/2}\,\min\{h_T\,\sigma^{1/2}\,\nu^{-1/2}, 1\} & ,\sigma > 0\,. \end{cases}$$

$$\theta_F := \begin{cases} \nu^{-1/2}\,h_F^{1/2} & ,\sigma = 0\,, \\ \nu^{-1/4}\,\sigma^{-1/4}\,\min\{h_F\,\sigma^{1/2}\,\nu^{-1/2}, 1\}^{1/2} & ,\sigma > 0\,. \end{cases}$$

Hence, it can be easily shown that the Clément interpolation operator satifies

Lemma 9 *For all* $T \in \mathcal{T}_h$, $F \in \mathcal{E}(T)$, $\boldsymbol{v} \in H^1(\Omega)^2$, *there holds*

$$\|\boldsymbol{v} - I_h\boldsymbol{v}\|_{0,T} \preceq \theta_T\,\|\boldsymbol{v}\|_{a,\widetilde{\omega}_T}, \tag{4.3}$$

$$\|\boldsymbol{v} - I_h\boldsymbol{v}\|_{0,F} \preceq \theta_F\,\|\boldsymbol{v}\|_{a,\widetilde{\omega}_F}, \tag{4.4}$$

$$\|I_h\boldsymbol{v}\|_{a,T} \preceq \|\boldsymbol{v}\|_{a,\widetilde{\omega}_T}. \tag{4.5}$$

PROOF. See Lemma 4 in [4]. □

4.2 The auxiliary problem

In what follows, the functions $\boldsymbol{e}$ and E stand for the velocity and the pressure approximation errors, i.e.,

$$\begin{aligned}\boldsymbol{e} &:= \boldsymbol{u} - \boldsymbol{u}_h\,,\\ E &:= p - p_h\,,\end{aligned}$$

which are indirectly estimated by the following auxiliary problem: *Find* $(\boldsymbol{\phi}, \psi) \in \boldsymbol{H} \times Q$ *such that*

$$a(\boldsymbol{\phi}, \boldsymbol{v}) + d(\psi, q) = a(\boldsymbol{e}, \boldsymbol{v}) + b(\boldsymbol{e}, q) + b(\boldsymbol{v}, E) + l(\boldsymbol{u}; \boldsymbol{u}_h, \boldsymbol{v}) \quad \forall (\boldsymbol{v}, q) \in \boldsymbol{H} \times Q, \tag{4.6}$$

where

$$l(\boldsymbol{u}; \boldsymbol{u}_h, \boldsymbol{v}) := c(\boldsymbol{u}; \boldsymbol{u}, \boldsymbol{v}) - c(\boldsymbol{u}_h; \boldsymbol{u}_h, \boldsymbol{v}).$$

Clearly, the well-posedeness of the above system arises from the ellipticity of $a(\cdot,\cdot)$ and $d(\cdot,\cdot)$ on $\boldsymbol{H}$ and Q, respectively.

Next, we establish an equivalence between the norms of $(\boldsymbol{e}, E) \in \boldsymbol{H} \times Q$ and the norms of the solution $(\boldsymbol{\phi}, \psi) \in \boldsymbol{H} \times Q$ of (4.6) which opens the door to design an error estimate based on the functions $(\boldsymbol{\phi}, \psi)$ only.

Theorem 10 *There exist positive constants* K_1 *and* K_2*, independent of* h*, such that*

$$K_1 \left\{ \|\boldsymbol{\phi}\|_a^2 + \|\psi\|_d^2 \right\} \leq \|\boldsymbol{e}\|_a^2 + \|E\|_d^2 \leq K_2 \left\{ \|\boldsymbol{\phi}\|_a^2 + \|\psi\|_d^2 \right\}.$$

PROOF. First, note that using (2.10) and (2.13), we have that for $\boldsymbol{v} \in \boldsymbol{H}$

$$\begin{aligned} l(\boldsymbol{u}; \boldsymbol{u}_h, \boldsymbol{v}) &= c(\boldsymbol{u}; \boldsymbol{u}, \boldsymbol{v}) - c(\boldsymbol{u}_h; \boldsymbol{u}_h, \boldsymbol{v}) \\ &= c(\boldsymbol{u}; \boldsymbol{e}, \boldsymbol{v}) + c(\boldsymbol{e}; \boldsymbol{u}_h, \boldsymbol{v}) \\ &\leq \beta \left\{ |\boldsymbol{u}|_{1,\Omega} |\boldsymbol{e}|_{1,\Omega} |\boldsymbol{v}|_{1,\Omega} + |\boldsymbol{e}|_{1,\Omega} |\boldsymbol{u}_h|_{1,\Omega} |\boldsymbol{v}|_{1,\Omega} \right\} \\ &\leq \beta \left\{ 2 |\boldsymbol{u}|_{1,\Omega} |\boldsymbol{e}|_{1,\Omega} |\boldsymbol{v}|_{1,\Omega} + |\boldsymbol{e}|_{1,\Omega}^2 |\boldsymbol{v}|_{1,\Omega} \right\} \\ &\leq \beta \left\{ 2\gamma \frac{\nu}{\beta} |\boldsymbol{e}|_{1,\Omega} |\boldsymbol{v}|_{1,\Omega} + |\boldsymbol{e}|_{1,\Omega}^2 |\boldsymbol{v}|_{1,\Omega} \right\} \\ &\leq \left\{ 2\gamma + \frac{\beta}{\nu} |\boldsymbol{e}|_{1,\Omega} \right\} \|\boldsymbol{e}\|_a \|\boldsymbol{v}\|_a. \end{aligned} \tag{4.7}$$

Furthermore, using (2.12) and following above steps closely it holds

$$l(\boldsymbol{u};\boldsymbol{u}_h,\boldsymbol{e}) \leq \left\{\gamma + \frac{\beta}{\nu}\left|\boldsymbol{e}\right|_{1,\Omega}\right\}\|\boldsymbol{e}\|_a^2. \tag{4.8}$$

Next, the upper and lower bound are addressed separately.

Upper bound: From equation (2.9) and setting $q = 0$ in (4.6), (2.7) and (4.7), there holds

$$\begin{aligned}\alpha_b\sqrt{\frac{\nu}{\sigma+\nu}}\,\|E\|_d &\leq \sup_{\boldsymbol{v}\in\boldsymbol{H}}\frac{|b(\boldsymbol{v},E)|}{\|\boldsymbol{v}\|_a}\\ &= \sup_{\boldsymbol{v}\in\boldsymbol{H}}\frac{|a(\boldsymbol{\phi},\boldsymbol{v}) - a(\boldsymbol{e},\boldsymbol{v}) - l(\boldsymbol{u};\boldsymbol{u}_h,\boldsymbol{v})\ |}{\|\boldsymbol{v}\|_a}\\ &\leq \|\boldsymbol{\phi}\|_a + \left\{3 + \frac{\beta}{\nu}\left|\boldsymbol{e}\right|_{1,\Omega}\right\}\|\boldsymbol{e}\|_a. \end{aligned}\tag{4.9}$$

In addition, by picking $q = 0$ and $\boldsymbol{v} = \boldsymbol{e}$ in (4.6) and using (4.8) we arrive at

$$\begin{aligned}\|\boldsymbol{e}\|_a^2 &= a(\boldsymbol{\phi},\boldsymbol{e}) - b(\boldsymbol{e},E) - l(\boldsymbol{u};\boldsymbol{u}_h,\boldsymbol{e})\\ &= a(\boldsymbol{\phi},\boldsymbol{e}) - d(\psi,E) - l(\boldsymbol{u};\boldsymbol{u}_h,\boldsymbol{e})\\ &\leq \|\boldsymbol{\phi}\|_a\|\boldsymbol{e}\|_a + \|\psi\|_d\|E\|_d + \left\{\gamma + \frac{\beta}{\nu}\left|\boldsymbol{e}\right|_{1,\Omega}\right\}\|\boldsymbol{e}\|_a^2, \end{aligned}\tag{4.10}$$

and we gather (4.9) and (4.10) to obtain

$$\begin{aligned}\|\boldsymbol{e}\|_a^2 \leq \frac{1}{\alpha_b}\sqrt{\frac{\sigma+\nu}{\nu}}\,\|\boldsymbol{\phi}\|_a\|\psi\|_d + \|\boldsymbol{e}\|_a\left\{\|\boldsymbol{\phi}\|_a + \frac{1}{\alpha_b}\sqrt{\frac{\sigma+\nu}{\nu}}\left(3 + \frac{\beta}{\nu}\left|\boldsymbol{e}\right|_{1,\Omega}\right)\|\psi\|_d\right\}\\ + \|\boldsymbol{e}\|_a^2\left\{\gamma + \frac{\beta}{\nu}\left|\boldsymbol{e}\right|_{1,\Omega}\right\}.\end{aligned}$$

Next, we assume $|\boldsymbol{e}|_{1,\Omega}$ to be sufficiently small in a way that there exists $\varepsilon > 0$ such that (see [36] for a related assumption)

$$\gamma + \frac{\varepsilon^2}{2} + \frac{\beta}{\nu}\left|\boldsymbol{e}\right|_{1,\Omega} =: \gamma' < 1. \tag{4.11}$$

The existence of such of ε along with the inequality $xy \leq \dfrac{\varepsilon^2 x^2}{2} + \dfrac{y^2}{2\,\varepsilon^2}$, for all $x, y > 0$, imply

$$
\begin{aligned}
\|\boldsymbol{e}\|_a^2 &\leq \frac{1}{\alpha_b}\sqrt{\frac{\sigma+\nu}{\nu}}\,\|\psi\|_d\|\boldsymbol{\phi}\|_a + \frac{\varepsilon^2}{2}\,\|\boldsymbol{e}\|_a^2 \\
&\quad + \frac{1}{2\varepsilon^2}\left\{\|\boldsymbol{\phi}\|_a + \frac{1}{\alpha_b}\sqrt{\frac{\sigma+\nu}{\nu}}\,\left(3+\frac{\beta}{\nu}\,|\boldsymbol{e}|_{1,\Omega}\right)\,\|\psi\|_d\right\}^2 \\
&\quad + \left\{\gamma + \frac{\beta}{\nu}|\boldsymbol{e}|_{1,\Omega}\right\}\|\boldsymbol{e}\|_a^2 \\
&= \frac{1}{\alpha_b}\sqrt{\frac{\sigma+\nu}{\nu}}\,\|\psi\|_d\|\boldsymbol{\phi}\|_a + \gamma'\,\|\boldsymbol{e}\|_a^2 \\
&\quad + \frac{1}{2\varepsilon^2}\left\{\|\boldsymbol{\phi}\|_a + \frac{1}{\alpha_b}\sqrt{\frac{\sigma+\nu}{\nu}}\,\left(3+\frac{\beta}{\nu}\,|\boldsymbol{e}|_{1,\Omega}\right)\,\|\psi\|_d\right\}^2 \\
&\leq \frac{1}{2\alpha_b}\sqrt{\frac{\sigma+\nu}{\nu}}\left[\|\psi\|_d^2 + \|\boldsymbol{\phi}\|_a^2\right] + \gamma'\,\|\boldsymbol{e}\|_a^2 \\
&\quad + \frac{1}{\varepsilon^2}\left\{\|\boldsymbol{\phi}\|_a^2 + \frac{1}{\alpha_b^2}\,\left(\frac{\sigma+\nu}{\nu}\right)\,\left(3+\frac{\beta}{\nu}\,|\boldsymbol{e}|_{1,\Omega}\right)^2\,\|\psi\|_d^2\right\} \\
&\leq \left[\frac{1}{2\alpha_b}\sqrt{\frac{\sigma+\nu}{\nu}} + \frac{1}{\varepsilon^2}\right]\|\boldsymbol{\phi}\|_a^2 + \gamma'\,\|\boldsymbol{e}\|_a^2 \\
&\quad + \frac{1}{\alpha_b}\sqrt{\frac{\sigma+\nu}{\nu}}\,\left\{\frac{1}{2} + \frac{1}{\varepsilon^2\alpha_b}\sqrt{\frac{\sigma+\nu}{\nu}}\left(3+\frac{\beta}{\nu}\,|\boldsymbol{e}|_{1,\Omega}\right)^2\right\}\,\|\psi\|_d^2\,.
\end{aligned}
$$

Now, from the previous inequality and (4.11) we get

$$
\begin{aligned}
\|\boldsymbol{e}\|_a^2 &\leq \frac{1}{1-\gamma'}\left[\frac{1}{2\alpha_b}\sqrt{\frac{\sigma+\nu}{\nu}} + \frac{1}{\varepsilon^2}\right]\|\boldsymbol{\phi}\|_a^2 \\
&\quad + \frac{1}{1-\gamma'}\sqrt{\frac{\sigma+\nu}{\nu}}\,\frac{1}{\alpha_b}\,\left\{\frac{1}{2} + \frac{1}{\varepsilon^2\alpha_b}\sqrt{\frac{\sigma+\nu}{\nu}}\left(3+\frac{\beta}{\nu}\,|\boldsymbol{e}|_{1,\Omega}\right)^2\right\}\,\|\psi\|_d^2\,.
\end{aligned}
$$

Finally, the upper bound follows from the above inequality and (4.9).

Lower bound: Taking $\boldsymbol{v} = \boldsymbol{\phi},$ and $q = 0$ in (4.6), and using (2.8) and (4.7), it holds

$$
\begin{aligned}
\|\boldsymbol{\phi}\|_a^2 &= a(\boldsymbol{\phi},\boldsymbol{\phi}) \\
&= a(\boldsymbol{e},\boldsymbol{\phi}) + b(\boldsymbol{\phi},E) + l(\boldsymbol{u},\boldsymbol{u}_h,\boldsymbol{\phi}) \\
&\leq \|\boldsymbol{e}\|_a\|\boldsymbol{\phi}\|_a + \sqrt{2}\,\|\boldsymbol{\phi}\|_a\|E\|_d + \left\{2\gamma + \frac{\beta}{\nu}\,|\boldsymbol{e}|_{1,\Omega}\right\}\,\|\boldsymbol{e}\|_a\|\boldsymbol{\phi}\|_a \\
&\leq \sqrt{2}\,\|\boldsymbol{\phi}\|_a\|E\|_d + \left\{3 + \frac{\beta}{\nu}\,|\boldsymbol{e}|_{1,\Omega}\right\}\,\|\boldsymbol{e}\|_a\|\boldsymbol{\phi}\|_a,
\end{aligned}
$$

then,

$$\|\boldsymbol{\phi}\|_a \leq \left\{3 + \frac{\beta}{\nu}\,|\boldsymbol{e}|_{1,\Omega}\right\}\,\|\boldsymbol{e}\|_a + \sqrt{2}\,\|E\|_d\,. \tag{4.12}$$

Next, setting $\boldsymbol{v} = \boldsymbol{0}$ and $q = \psi$ in (4.6), and using (2.8), we end up with

$$\|\psi\|_d^2 \,=\, d(\psi,\psi) \,=\, b(\boldsymbol{e},\psi) \,\leq\, \sqrt{2}\,\|\boldsymbol{e}\|_a\|\psi\|_d \,\leq\, \|\boldsymbol{e}\|_a^2 + \frac{1}{2}\,\|\psi\|_d^2\,,$$

which implies

$$\|\psi\|_d^2 \leq 2\,\|\boldsymbol{e}\|_a^2\,. \tag{4.13}$$

Hence, we gather (4.12) and (4.13) to get

$$\|\boldsymbol{\phi}\|_a^2 + \|\psi\|_d^2 \,\leq\, 2\,\left[1 + \left\{3 + \frac{\beta}{\nu}\,|\boldsymbol{e}|_{1,\Omega}\right\}^2\right]\,\|\boldsymbol{e}\|_a^2 + 4\,\|E\|_d^2\,.$$

Finally, from the bound (4.11) for ε, the following inequality holds

$$3 + \frac{\varepsilon^2}{2} + \frac{\beta}{\nu}\,|\boldsymbol{e}|_{1,\Omega} \leq 4\,,$$

and, thus, we obtain

$$\|\boldsymbol{\phi}\|_a^2 + \|\psi\|_d^2 \leq 34\left\{\|\boldsymbol{e}\|_a^2 + \|E\|_d^2\right\},$$

and the result follows. $\square$

From the definition of $\boldsymbol{e}$ and E, the auxiliar problem (4.6) is equivalent to

$$a(\boldsymbol{\phi},\boldsymbol{v}) + d(\psi,q) = (\boldsymbol{f},\boldsymbol{v})_\Omega - a(\boldsymbol{u}_h,\boldsymbol{v}) - b(\boldsymbol{u}_h,q) - b(\boldsymbol{v},p_h) - c(\boldsymbol{u}_h;\boldsymbol{u}_h,\boldsymbol{v}) \tag{4.14}$$

for all $(\boldsymbol{v},q)$ in $\boldsymbol{H}\times Q$. It can be rewritten, for sake of compactness, as

$$a(\boldsymbol{\phi},\boldsymbol{v}) + d(\psi,q) = \mathcal{R}_h(\boldsymbol{v},q) \qquad \forall (\boldsymbol{v},q)\in \boldsymbol{H}\times Q\,, \tag{4.15}$$

where the right hand side $\mathcal{R}_h \in (\boldsymbol{H}\times Q)'$ stands for the residual functional given by

$$\mathcal{R}_h(\boldsymbol{v},q) := (\boldsymbol{f},\boldsymbol{v})_\Omega - a(\boldsymbol{u}_h,\boldsymbol{v}) - b(\boldsymbol{u}_h,q) - b(\boldsymbol{v},p_h) - c(\boldsymbol{u}_h;\boldsymbol{u}_h,\boldsymbol{v})\,.$$

Remark 11 *The auxiliar problem (4.6) is decoupled. In fact, if one set* $\boldsymbol{v} = \boldsymbol{0}$ *in (4.14), then problem (4.6) becomes*

$$d(\psi, q) = -b(\boldsymbol{u}_h, q)\,, \tag{4.16}$$

which leads to

$$\psi = \nu \operatorname{div} \boldsymbol{u}_h\,. \tag{4.17}$$

Hence, if we pick in the sequel the test functions $(\boldsymbol{v}, 0)$ *in (4.14) we arrive at*

$$a(\boldsymbol{\phi}, \boldsymbol{v}) = \mathcal{R}_h^1(\boldsymbol{v}), \tag{4.18}$$

where $\mathcal{R}_h^1 \in \boldsymbol{H}'$ *reads*

$$\mathcal{R}_h^1(\boldsymbol{v}) := (\boldsymbol{f}, \boldsymbol{v})_\Omega - a(\boldsymbol{u}_h, \boldsymbol{v}) - b(\boldsymbol{v}, p_h) - c(\boldsymbol{u}_h; \boldsymbol{u}_h, \boldsymbol{v})\,.$$

□

An equivalent and useful expression for $\mathcal{R}_h^1$ arises using integration by parts which leads to

$$\mathcal{R}_h^1(\boldsymbol{v}) \;=\; \sum_{T\in\mathcal{T}_h} (\boldsymbol{R}_T, \boldsymbol{v})_T + \sum_{F\in\mathcal{E}_\Omega} (\boldsymbol{R}_F, \boldsymbol{v})_F\,,$$

where $\boldsymbol{R}_T \in L^2(T)^2$ and $\boldsymbol{R}_F \in L^2(F)^2$ are given by

$$\boldsymbol{R}_T := (\boldsymbol{f} + \nu\,\Delta\boldsymbol{u}_h - \nabla p_h - (\nabla\boldsymbol{u}_h)\boldsymbol{u}_h - \sigma\,\boldsymbol{u}_h)|_T\,,$$

and

$$\boldsymbol{R}_F \;:=\; -\,[\![\boldsymbol{\varepsilon}_h \cdot \boldsymbol{n}]\!]_F\,.$$

Here $\boldsymbol{\varepsilon}_h := \nu\,\nabla\boldsymbol{u}_h - p_h\,\boldsymbol{I}$ (where $\boldsymbol{I}$ stands for the $\mathbb{R}^{2\times 2}$ identity matrix), and thus, it is worth noting that, as p_h is a continuous function in Ω, the residual on the edges $\boldsymbol{R}_F$ reduces to $-[\![\nu\nabla\boldsymbol{u}_h \cdot \boldsymbol{n}_F]\!]_F$. The following technical result will be useful in the forthcoming proofs.

Lemma 12 *For all* $\boldsymbol{v}_h \in \boldsymbol{H}_h$ *there holds*

$$\mathcal{R}_h^1(\boldsymbol{v}_h) \preceq \sum_{T\,\in\,\mathcal{T}_h} \left[\theta_T\,\|\boldsymbol{R}_T\|_{0,T} + \nu^{-1/2}\,h_T\,\|\boldsymbol{u}_h\|_{\infty,T}\|\operatorname{div}\boldsymbol{u}_h\|_{0,T}\right] \|\boldsymbol{v}_h\|_{a,T}\,.$$

PROOF. From the definition of $\mathcal{R}_h^1$ and using (3.14) with $q_h = 0$, there holds

$$\begin{aligned}
\mathcal{R}_h^1(\boldsymbol{v}_h) &= (\boldsymbol{f}, \boldsymbol{v}_h)_\Omega - a(\boldsymbol{u}_h, \boldsymbol{v}_h) - b(\boldsymbol{v}_h, p_h) - c(\boldsymbol{u}_h; \boldsymbol{u}_h, \boldsymbol{v}) \\
&= -\sum_{T\,\in\,\mathcal{T}_h} \Big(\boldsymbol{R}_T, \tau_T\left[(\nabla\boldsymbol{v}_h)\boldsymbol{u}_h + \nu\,\Delta\boldsymbol{v}_h - \sigma\,\boldsymbol{v}_h\right]\Big)_T \\
&\quad + \sum_{T\,\in\,\mathcal{T}_h} (\operatorname{div}\boldsymbol{u}_h, \delta_T \operatorname{div}\boldsymbol{v}_h)_T.
\end{aligned}$$

Next, from Hölder inequality and Lemma 4 it follows

$$\begin{aligned}|(\boldsymbol{R}_T, \tau_T\,(\nabla \boldsymbol{v}_h)\boldsymbol{u}_h)_T| &\leq \int_T |\tau_T|\,|\boldsymbol{R}_T(\nabla \boldsymbol{v}_h)\boldsymbol{u}_h| \\ &\leq |\tau_T|\,\|\boldsymbol{R}_T\|_{0,T}\,\|\nabla \boldsymbol{v}_h\|_{0,T}\|\boldsymbol{u}_h\|_{\infty,T} \\ &\preceq |\tau_T|\,h_T^{-1}\,\theta_T\,\|\boldsymbol{R}_T\|_{0,T}\,\|\boldsymbol{v}_h\|_{a,T}\|\boldsymbol{u}_h\|_{\infty,T} \\ &\preceq \theta_T\,\|\boldsymbol{R}_T\|_{0,T}\|\boldsymbol{v}_h\|_{a,T}\,,\end{aligned}$$

and we can similarly deduce that

$$|(\boldsymbol{R}_T, \tau_T\,\nu\,\Delta \boldsymbol{v}_h)_T| \preceq \theta_T\,\|\boldsymbol{R}_T\|_{0,T}\|\boldsymbol{v}_h\|_{a,T},$$

and

$$|(\boldsymbol{R}_T, \tau_T\,\sigma\,\boldsymbol{v}_h)_T| \leq \theta_T\,\|\boldsymbol{R}_T\|_{0,T}\|\boldsymbol{v}_h\|_{a,T}.$$

On the other hand, using (3.21) and Cauchy-Schwarz's inequality, it holds

$$\begin{aligned}(\operatorname{div}\boldsymbol{u}_h, \delta_T \operatorname{div}\boldsymbol{v}_h)_T &\leq \int_T |\delta_T \operatorname{div}\boldsymbol{u}_h \operatorname{div}\boldsymbol{v}_h| \\ &\preceq \nu^{-1/2}\,h_T\,\|\boldsymbol{u}_h\|_{\infty,T}\|\operatorname{div}\boldsymbol{u}_h\|_{0,T}\|\boldsymbol{v}_h\|_{a,T}.\end{aligned}$$

Finally, gathering overall estimates the result follows. □

Remark 13 *The characterization of ψ given in (4.17) replaced in Theorem 10 leads to the following equivalence result*

$$K_1\left\{\|\boldsymbol{\phi}\|_a^2 + \nu\,\|\operatorname{div}\boldsymbol{u}_h\|_{0,\Omega}^2\right\} \preceq \|\boldsymbol{e}\|_a^2 + \|E\|_d^2 \preceq K_2\left\{\|\boldsymbol{\phi}\|_a^2 + \nu\,\|\operatorname{div}\boldsymbol{u}_h\|_{0,\Omega}^2\right\}. \tag{4.19}$$

Therefore, the a posteriori error estimator would demand to evaluate $\|\boldsymbol{\phi}\|_a$ only. Such idea is pursued in the next section. □

4.3 The hierarchical error estimator

Following closely the idea of [4], let $\boldsymbol{W}_h$ be a finite element space such that $\boldsymbol{H}_h \subseteq \boldsymbol{W}_h \subseteq \boldsymbol{H}$. Let us suppose that there exist M subspaces $\boldsymbol{H}_i$ of $\boldsymbol{W}_h$ such that

$$\boldsymbol{W}_h = \boldsymbol{H}_0 + \sum_{i=1}^{M} \boldsymbol{H}_i\,,$$

where $\boldsymbol{H}_0 := \boldsymbol{H}_h$. Associated with each subspace $\boldsymbol{H}_i$ a projection operator $P_i : \boldsymbol{H} \longrightarrow \boldsymbol{H}_i$ is built from the solution of the local problem

$$a(P_i\boldsymbol{v}, \boldsymbol{w}_i) = a(\boldsymbol{v}, \boldsymbol{w}_i) \qquad \forall \boldsymbol{w}_i \in \boldsymbol{H}_i\,, P_i\boldsymbol{v} \in \boldsymbol{H}_i\,.$$

Next, we define the a posteriori error estimator η_H by

$$\eta_H := \left\{ \sum_{i=1}^{M} a(P_i\boldsymbol{\phi}, P_i\boldsymbol{\phi}) \right\}^{1/2},$$

where $\boldsymbol{\phi}$ is the solution of (4.18), and we recall that $P_i\boldsymbol{\phi}$ is the solution of the local problem: *Find* $P_i\boldsymbol{\phi} \in \boldsymbol{H}_i$ *such that*

$$a(P_i\boldsymbol{\phi}, \boldsymbol{v}_i) \;=\; \mathcal{R}_h^1(\boldsymbol{v}_i) \qquad \forall \boldsymbol{v}_i \in \boldsymbol{H}_i\,.$$

In the seek for low cost computations, spaces $\boldsymbol{H}_i$ are made local by associating them to each element $T \in \mathcal{T}_h$ and each edge $F \in \mathcal{E}_\Omega$. From such construction, the error estimator η_H decomposes as

$$\eta_H = \left\{ \sum_{T\in\mathcal{T}_h} a(P_T\boldsymbol{\phi}, P_T\boldsymbol{\phi}) + \sum_{F\in\mathcal{E}_\Omega} a(P_F\boldsymbol{\phi}, P_F\boldsymbol{\phi}) \right\}^{1/2}. \tag{4.20}$$

The next step consists of choosing appropriated spaces $\boldsymbol{H}_i$. This is accomplished by assuming $\boldsymbol{H}_i$ spanned by bubble functions $\boldsymbol{H}^b$ requiring two ingredients: First, the spaces $\boldsymbol{H}^b$ split as

$$\boldsymbol{H}^b = \begin{cases} \boldsymbol{H}^b_T & \text{for each } T \in \mathcal{T}_h, \\ \boldsymbol{H}^b_F & \text{for each } F \in \mathcal{E}_\Omega\,, \end{cases}$$

where $\boldsymbol{H}^b_T \subset H^1_0(T)^2$ and $\boldsymbol{H}^b_F \subset H^1_0(\omega_F)^2$. Moreover, those bubble spaces are affine–equivalent to a finite dimensional space on a reference configuration, so that the following estimate holds

$$\|\mathbf{b}\|^2_{0,T} \;\preceq\; h_T^2\,|\mathbf{b}|^2_{1,T}\,,$$

for all $\mathbf{b} \in \boldsymbol{H}^b$, and all $T \in \mathcal{T}_h$.

Secondly, those bubble spaces fulfill the following inf-sup conditions (LBB): *There exists* $\beta^* > 0$*, independent of* h*,* σ *and* ν*, such that*

$$\sup_{b_T \in \boldsymbol{H}^b_T} \frac{(b_T, \boldsymbol{R}_T)_T}{\|b_T\|_{a,T}} \geq \beta^* \, \theta_T \|\boldsymbol{R}_T\|_{0,T} \qquad \forall T \in \mathcal{T}_h \,,$$

$$\sup_{b_F \in \boldsymbol{H}^b_F} \frac{(b_F, \boldsymbol{R}_F)_F}{\|b_F\|_{a,\omega_F}} \geq \beta^* \, \theta_F \|\boldsymbol{R}_F\|_{0,F} \qquad \forall F \in \mathcal{E}_\Omega \,,$$

where $\|\cdot\|_{a,D}$ stands for the norm induced by the bilinear for $a(\cdot,\cdot)$ over the set $D \subseteq \mathbb{R}^2$.

Remark 14 *As an example of bubble functions satisfying the (LBB) conditions we have the standard polinomyals bubbles based on the barycentric coordinates of each element $T \in \mathcal{T}_h$ (for further details see Appendix B in [4]).* □

The next result is recalled as it is needed for the proof of the reliability.

Lemma 15 *Suppose the (LBB) holds. Then,*

$$\begin{aligned}\mathcal{R}^1_h(\boldsymbol{v}) \preceq & \sum_{T \in \mathcal{T}_h} a(P_T\boldsymbol{\phi}, P_T\boldsymbol{\phi})^{1/2} \theta_T^{-1} \|\boldsymbol{v}\|_{0,T} \\ & + \sum_{F \in \mathcal{E}_\Omega} \left[a(P_F\boldsymbol{\phi}, P_F\boldsymbol{\phi})^{1/2} + \sum_{T' \subset \omega_F} a(P_{T'}\boldsymbol{\phi}, P_{T'}\boldsymbol{\phi})^{1/2} \right] \theta_F^{-1} \, \|\boldsymbol{v}\|_{0,F},\end{aligned}$$

for all $\boldsymbol{v}$ in $\boldsymbol{H}$.

PROOF. See Lemma 12 in [4]. □

We are ready to prove the reliability of the error estimator.

Lemma 16 *Let $\boldsymbol{\phi}$ be the solution of (4.18). If the (LBB) holds, then*

$$\|\boldsymbol{\phi}\|_a^2 \preceq \eta_H^2 + \sum_{T \in \mathcal{T}_h} \nu^{-1} h_T^2 \, \|\boldsymbol{u}_h\|^2_{\infty,T} \|\mathrm{div}\, \boldsymbol{u}_h\|^2_{0,T} \,.$$

PROOF. From Lemma 15 with $\boldsymbol{v} = \boldsymbol{\phi} - I_h\boldsymbol{\phi}$, Cauchy-Schwarz's inequality and Lemma 9, there holds

$$
\begin{aligned}
\mathcal{R}_h^1(\boldsymbol{\phi} - I_h\boldsymbol{\phi}) &\preceq \sum_{T\in\mathcal{T}_h} a(P_T\boldsymbol{\phi}, P_T\boldsymbol{\phi})^{1/2}\theta_T^{-1}\|\boldsymbol{\phi} - I_h\boldsymbol{\phi}\|_{0,T} \\
&+ \sum_{F\in\mathcal{E}_\Omega}\Big[a(P_F\boldsymbol{\phi}, P_F\boldsymbol{\phi})^{1/2} + \sum_{T'\subset\omega_F} a(P_{T'}\boldsymbol{\phi}, P_{T'}\boldsymbol{\phi})^{1/2}\Big]\theta_F^{-1}\|\boldsymbol{\phi} - I_h\boldsymbol{\phi}\|_{0,F} \\
&\preceq \left\{\sum_{T\in\mathcal{T}_h} a(P_T\boldsymbol{\phi}, P_T\boldsymbol{\phi}) + \sum_{F\in\mathcal{E}_\Omega} a(P_F\boldsymbol{\phi}, P_F\boldsymbol{\phi})\right\}^{1/2} \cdot \\
&\left\{\sum_{T\in\mathcal{T}_h} \theta_T^{-2}\|\boldsymbol{\phi} - I_h\boldsymbol{\phi}\|_{0,T}^2 + \sum_{F\,\in\,\mathcal{E}_\Omega} \theta_F^{-2}\|\boldsymbol{\phi} - I_h\boldsymbol{\phi}\|_{0,F}^2\right\}^{1/2} \\
&\preceq \left\{\sum_{T\in\mathcal{T}_h} a(P_T\boldsymbol{\phi}, P_T\boldsymbol{\phi}) + \sum_{F\in\mathcal{E}_\Omega} a(P_F\boldsymbol{\phi}, P_F\boldsymbol{\phi})\right\}^{1/2} \|\boldsymbol{\phi}\|_a. \qquad (4.21)
\end{aligned}
$$

On the other hand, using Cauchy-Schwarz's inequality, the (LBB) condition and the definition of $P_T\boldsymbol{\phi}$ we obtain

$$
\begin{aligned}
\theta_T\|\boldsymbol{R}_T\|_{0,T} &\leq \frac{1}{\beta^*}\sup_{b_T\,\in\,\boldsymbol{H}_T^b}\frac{(b_T, \boldsymbol{R}_T)_T}{\|b_T\|_{a,T}} = \frac{1}{\beta^*}\sup_{b_T\,\in\,\boldsymbol{H}_T^b}\frac{\mathcal{R}_h^1(b_T)}{b_T\|_{a,T}} \\
&= \frac{1}{\beta^*}\sup_{b_T\,\in\,\boldsymbol{H}_T^b}\frac{a(P_T\boldsymbol{\phi}, b_T)}{\|b_T\|_{a,T}} \;\leq\; \frac{1}{\beta^*}\,\|P_T\boldsymbol{\phi}\|_{a,T}\,. \qquad (4.22)
\end{aligned}
$$

Now, from Lemmas 12 and 15, (4.21), (4.22), (4.5) and Cauchy-Schwarz's inequality, it comes that

$$
\begin{aligned}
\|\boldsymbol{\phi}\|_a^2 &= a(\boldsymbol{\phi}, \boldsymbol{\phi}) = \mathcal{R}_h^1(\boldsymbol{\phi}) \\
&= \mathcal{R}_h^1(\boldsymbol{\phi} - I_h\,\boldsymbol{\phi}) + \mathcal{R}_h^1(I_h\boldsymbol{\phi}) \\
&\preceq \left\{\sum_{T\in\mathcal{T}_h} a(P_T\boldsymbol{\phi}, P_T\boldsymbol{\phi}) + \sum_{F\in\mathcal{E}_\Omega} a(P_F\boldsymbol{\phi}, P_F\boldsymbol{\phi})\right\}^{1/2} \|\boldsymbol{\phi}\|_a + \\
&\sum_{T\,\in\,\mathcal{T}_h} \theta_T\,\|\boldsymbol{R}_T\|_{0,T}\|I_h\boldsymbol{\phi}\|_{a,T} + \sum_{T\,\in\,\mathcal{T}_h} \nu^{-1/2}h_T\,\|\boldsymbol{u}_h\|_{\infty,T}\|\mathrm{div}\,\boldsymbol{u}_h\|_{0,T}\|I_h\boldsymbol{\phi}\|_{a,T} \\
&\preceq \left\{\sum_{T\in\mathcal{T}_h} a(P_T\boldsymbol{\phi}, P_T\boldsymbol{\phi}) + \sum_{F\in\mathcal{E}_\Omega} a(P_F\boldsymbol{\phi}, P_F\boldsymbol{\phi})\right\}^{1/2} \|\boldsymbol{\phi}\|_a + \\
&\sum_{T\,\in\,\mathcal{T}_h} a(P_T\boldsymbol{\phi}, P_T\boldsymbol{\phi})^{1/2}\|\boldsymbol{\phi}\|_{a,\widetilde{\omega}_T} + \sum_{T\,\in\,\mathcal{T}_h} \nu^{-1/2}h_T\,\|\boldsymbol{u}_h\|_{\infty,T}\|\mathrm{div}\,\boldsymbol{u}_h\|_{0,T}\|\boldsymbol{\phi}\|_{a,\widetilde{\omega}_T} \\
&\preceq \left\{\sum_{T\in\mathcal{T}_h} a(P_T\boldsymbol{\phi}, P_T\boldsymbol{\phi}) + \sum_{F\in\mathcal{E}_\Omega} a(P_F\boldsymbol{\phi}, P_F\boldsymbol{\phi})\right\}^{1/2} \|\boldsymbol{\phi}\|_a \\
&+ \sum_{T\,\in\,\mathcal{T}_h} \nu^{-1/2}h_T\,\|\boldsymbol{u}_h\|_{\infty,T}\|\mathrm{div}\,\boldsymbol{u}_h\|_{0,T}\|\boldsymbol{\phi}\|_{a,\widetilde{\omega}_T}\,,
\end{aligned}
$$

and the result follows. □

From the previous results we can state the following equivalence theorem.

Theorem 17 *Let $\boldsymbol{\phi}$ be the solution of (4.18), and assume the (LBB) holds. Then*

$$\eta_H^2 \preceq \|\boldsymbol{\phi}\|_a^2 \preceq \eta_H^2 + \sum_{T\in\mathcal{T}_h} \nu^{-1} h_T^2 \,\|\boldsymbol{u}_h\|_{\infty,T}^2 \|\operatorname{div}\boldsymbol{u}_h\|_{0,T}^2,$$

where η_H is given by (4.20).

PROOF. The upper bound has been stated in Lemma 16. For the lower bound see Theorem 15 in [4]. □

Finally, we come up with the main result of this work. From (4.19) and Theorem 17, the finite element error can be estimated as follows.

Theorem 18 *Let $(\boldsymbol{u},p)$, $(\boldsymbol{u}_h,p_h)$ and $\boldsymbol{\phi}$ be the solutions of (2.1), (4.13) and (4.18), respectively, and suppose that the (LBB) holds. Then, the following equivalence holds*

$$K_1 \sum_{T\in\mathcal{T}_h} \tilde{\eta}_{H,T}^2 \preceq \|\boldsymbol{u}-\boldsymbol{u}_h\|_a^2+\|p-p_h\|_d^2 \preceq K_2 \sum_{T\in\mathcal{T}_h} \left[\tilde{\eta}_{H,T}^2+\nu^{-1}\, h_T^2\,\|\boldsymbol{u}_h\|_{\infty,T}^2\|\operatorname{div}\boldsymbol{u}_h\|_{0,T}^2\right],$$

where

$$\tilde{\eta}_{H,T} := \left\{ \|P_T\boldsymbol{\phi}\|_{a,T}^2 + \frac{1}{2} \sum_{F\in\mathcal{E}(T)\cap\mathcal{E}_\Omega} \|P_F\boldsymbol{\phi}\|_{a,F}^2 + \nu\,\|\operatorname{div}\boldsymbol{u}_h\|_{0,T}^2 \right\}^{1/2}. \qquad (4.23)$$

Remark 19 *It is worth stressing that the previous results holds without having assumed any saturation condition.* □

5 Numerical experiments

The adaptive scheme based on the *a posteriori* error estimator (4.23) and the unusual stabilized finite element (3.14) are tested. Its ability to recover accurate discrete solution without using a highly refined uniform mesh is validated through three numerical experiments.

The first test concerns with the validation of theoretical results related to the reliability and efficiency of the error estimator. To accomplish that, we adopt an analytical solution as reference, and we compare the exact finite element error to the estimated error. Afterward, no available analytical solutions exist for the remaining two tests and so the adaptive finite element scheme is

validated upon priori knowledge of the solution behavior. Overall numerical results used equal-order $[\mathbb{P}_1]^2 \times \mathbb{P}_1$ elements.

The adaptive procedure treated the nonlinearity by a Newton algorithm [35] and initiate the process using a quasi-uniform mesh. At each step, we compute the local error estimators $\tilde{\eta}_{H,T}$ for all T over the previous mesh $\mathcal{T}_h$, and refine those elements $T \in \mathcal{T}_h$ accordingly to

$$\tilde{\eta}_{H,T} \geq \theta \max\{\tilde{\eta}_{H,T} : \ T \in \mathcal{T}_h\} ,$$

where $\theta \in (0,1)$ is a prescribed parameter.

Compute numerical approximations of complex flows when $\nu \ll 1$ demanded a continuation strategy [29] on the Reynolds number. In general, the process initiated assuming $\nu = 1$. When it came to adapt meshes, we used the solution computed (after having been priorly interpolated on the current mesh [37]) on the previous mesh and set it as the guess solution for the Newton iteration method on the current mesh.

For practical purposes, we used the software `Triangle` to generated adapted meshes, as it allowed us to create successively refined meshes based on a hybrid Delaunay refinement algorithm. This process provided a sequence of refined meshes that form a hierarchy of nodes, but not a hierarchy of elements (for details, see [39]).

5.1 An analytical solution

The domain is $\Omega = (0,1) \times (0,1)$ and $\boldsymbol{f}$ is such that the exact solution of the problem (P) reads

$$\begin{aligned} u_1(x,y) &= -256x^2(x-1)^2y(y-1)(2y-1) , \\ u_2(x,y) &= -u_1(y,x) , \\ p(x,y) &= 150(x-0.5)(y-0.5) . \end{aligned}$$

The effectivity index defined by

$$E_i := \frac{\tilde{\eta}_H}{\|(\boldsymbol{u} - \boldsymbol{u}_h, p - p_h)\|} ,$$

is expected to remain bounded as h goes to 0 through a sequence of uniform meshes. The next two subsections are dedicated to validate theoretical results on asymptotic limit cases.

5.1.1 First case: $\sigma = 0$

First, we validate the stabilized scheme (3.14) with $\nu = 1$ and we show that it recovers the right orders of convergence and the effectivity index E_i stays bounded and close to one when $h \to 0$ (see Figure 1 and Table 1). Next, we perform the same test with $\nu = 10^{-4}$ and point out the robustness of methodology with respect to physical coefficients. Actually, no fundamental differences appears in Figure 2 and Table 2 when we compare them to the one obtained from the first case.

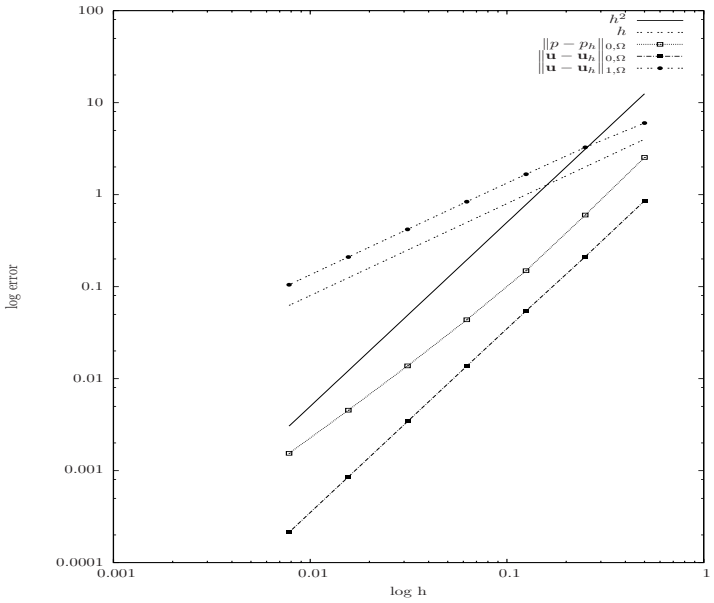

Fig. 1. Convergence history for $\nu = 1$ and $\sigma = 0$.

d.o.f	$\|(\boldsymbol{u} - \boldsymbol{u}_h, p - p_h)\|$	$\tilde{\eta}_H$	E_i
39	6.86325	5.20547	0.75845
123	3.30873	2.89566	0.87515
435	1.67288	1.53124	0.91533
1635	0.83904	0.77726	0.92637
6339	0.41972	0.39306	0.93647
24963	0.20985	0.19765	0.94185
99075	0.10491	0.09914	0.94500

Table 1
Exact error, a posteriori error estimator and effectivity index for $\nu = 1$ and $\sigma = 0$.

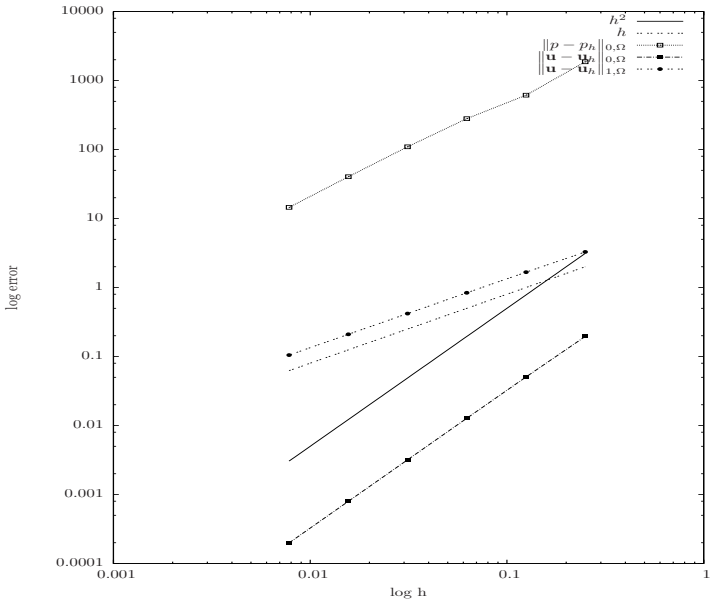

Fig. 2. Convergence history for $\nu = 10^{-4}$ and $\sigma = 0$.

d.o.f	$\|(\boldsymbol{u} - \boldsymbol{u}_h, p - p_h)\|$	$\tilde{\eta}_H$	E_i
39	652.07909	519.84385	0.79720
123	328.23434	287.19127	0.87495
435	167.04374	152.30331	0.91175
1635	83.87648	77.51751	0.92418
6339	41.96924	39.24102	0.93499
24963	20.98523	19.73516	0.94043
99075	10.49190	9.90076	0.94365

Table 2
Exact error, a posteriori error estimator and effectivity index for $\nu = 10^{-4}$ and $\sigma = 0$.

5.1.2 Second case: $\sigma = 1$

Now, we reveal the zeroth order term influence on numerical results and its impact on the adaptive strategy. We repeat the two tests used in the previous case, and we note that both the stabilized scheme and the adaptive procedure behaves as predicted by the theory.

In Figures 3 and 4 we depict the convergence curves of the stabilized scheme for different values of ν, and in Tables 3 and 4 the effectivity indexes are highlighted for both cases. It is worth noting that the values are asymptotically bounded and close to one.

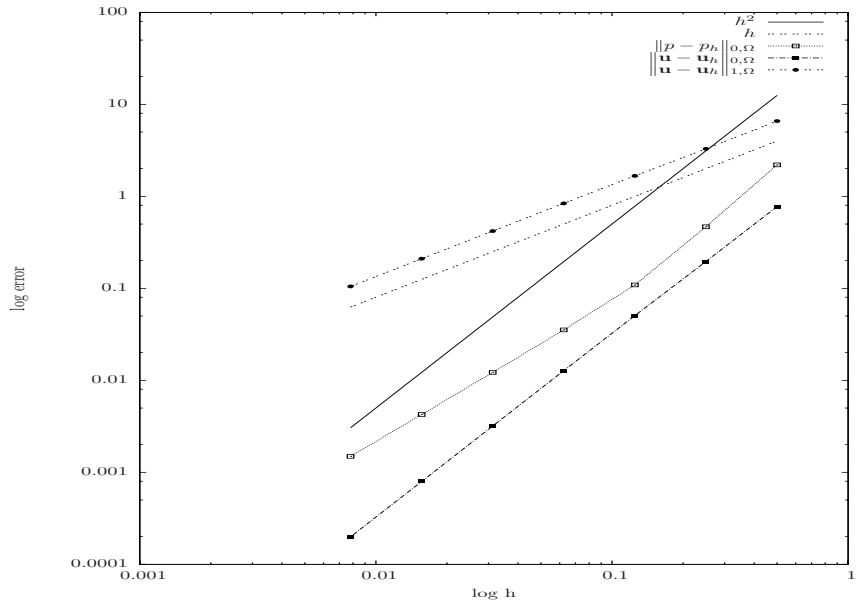

Fig. 3. Convergence history for $\nu = 1$ and $\sigma = 1$.

d.o.f	$\|(\boldsymbol{u} - \boldsymbol{u}_h, p - p_h)\|$	$\tilde{\eta}_H$	E_i
39	6.88932	5.33808	0.77483
123	3.31042	2.90868	0.87864
435	1.67286	1.53223	0.91593
1635	0.83904	0.77739	0.92652
6339	0.41972	0.39308	0.93651
24963	0.20985	0.19765	0.94186
99075	0.10491	0.09914	0.94500

Table 3
Exact error, a posteriori error estimator and effectivity index for $\nu = 1$ and $\sigma = 1$.

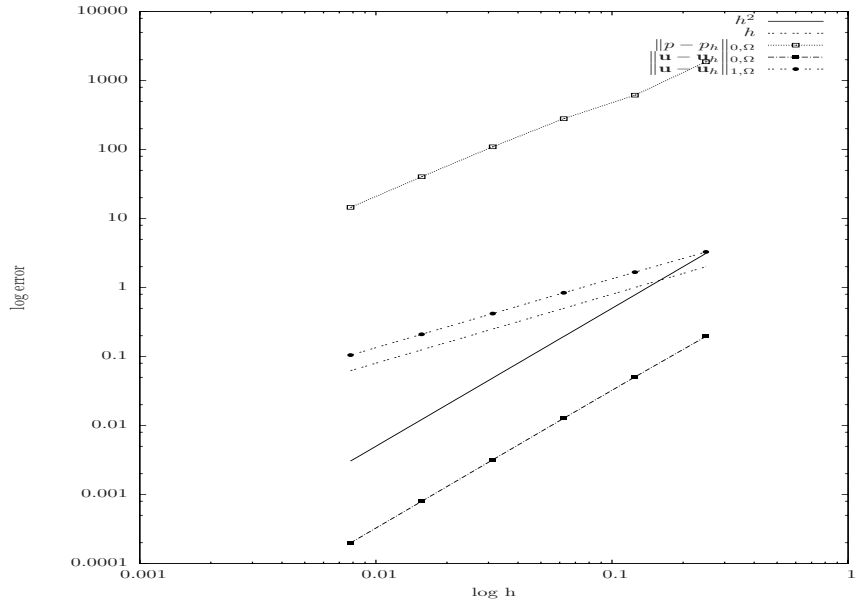

Fig. 4. Convergence history for $\nu = 10^{-4}$ and $\sigma = 1$.

d.o.f	$\|(\boldsymbol{u} - \boldsymbol{u}_h, p - p_h)\|$	$\tilde{\eta}_H$	E_i
39	652.07909	519.84435	0.79721
123	328.23434	287.19131	0.87495
435	167.04374	152.30331	0.91175
1635	83.87648	77.51751	0.92418
6339	41.96924	39.24102	0.93499
24963	20.98523	19.73516	0.94043
99075	10.49190	9.90076	0.94365

Table 4
Exact error, a posteriori error estimator and effectivity index for $\nu = 10^{-4}$ and $\sigma = 1$.

5.2 The lid-driven cavity problem

The lid-driven cavity is a standard test problem to validate numerical methods in fluid (see, for instance [27] and [41]). Details defining the problem are depicted in Figure 5. The source function is set as $\boldsymbol{f} = \boldsymbol{0}$.

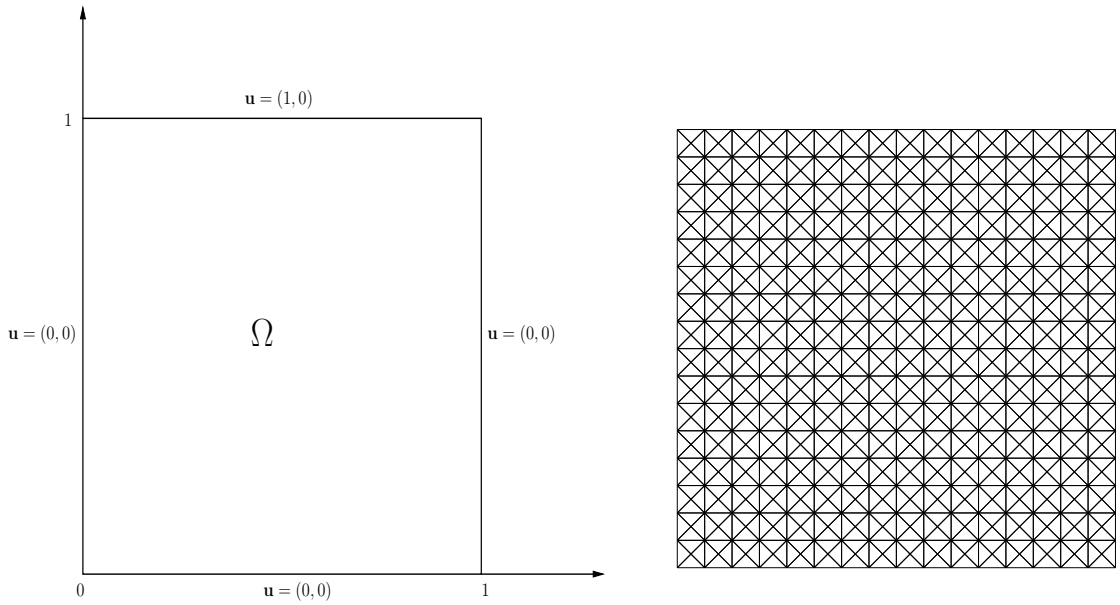

Fig. 5. Boundary conditions for the lid-driven cavity problem and the initial mesh.

5.2.1 First case: $\sigma = 0$

We consider first the case $\nu = 1$. Due to the change of boundary conditions, two singularities appears at the top corners of the domain. Figure 6 shows the final adapted mesh as well as the streamline contours associated with such mesh. As expected, the error estimator lead elements to be concentrated around the singularities.

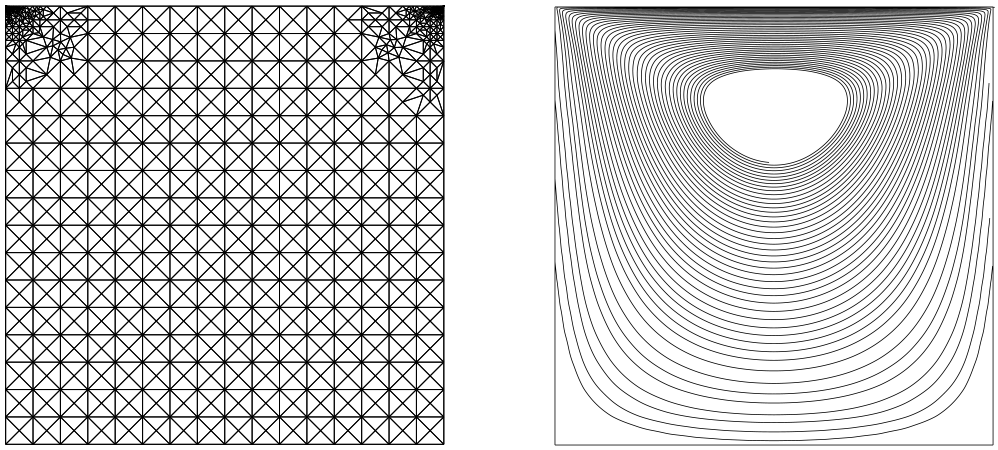

Fig. 6. Lid–Driven Cavity problem for $\nu = 1$ and $\sigma = 0$. Adaptive mesh and streamlines. The number of nodes of the mesh is 1.526 nodes.

Next, we set $\nu = 1/5000$. In addition to the two corner singularities, now the exact solution exhibits a complex vorticitity field. The error estimator behavior is remarkable as the mesh captures the phenomena as shown in Figure 7.

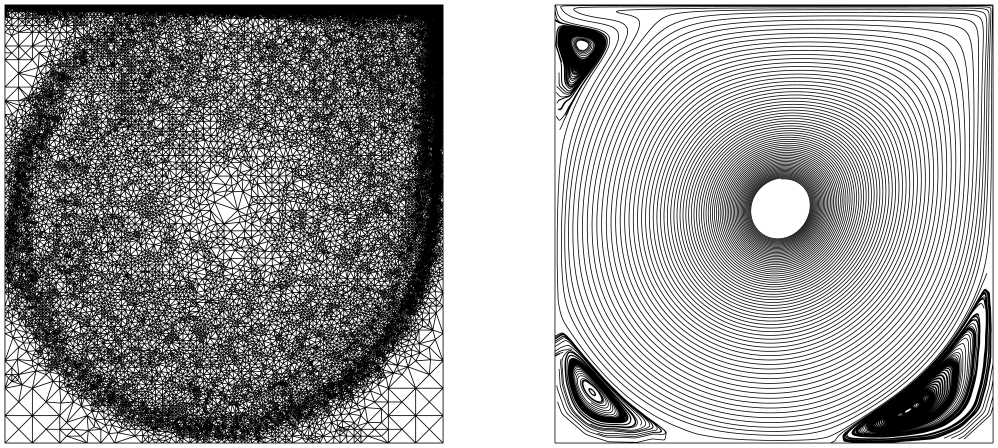

Fig. 7. Lid–Driven Cavity problem for $\nu = 1/5000$ and $\sigma = 0$. Adaptive mesh and streamlines. The number of nodes of the mesh is 37.038 nodes.

5.2.2 Second case: $\sigma = 1$

The value of the diffusivity coefficients are $\nu = 10^{-2}$ and $\nu = 10^{-3}$. The pattern showed by both flows are different from the previous example as reactive boundary layers show up. They are captured by the error estimator as points out the adaptive process in Figures 8 and 9.

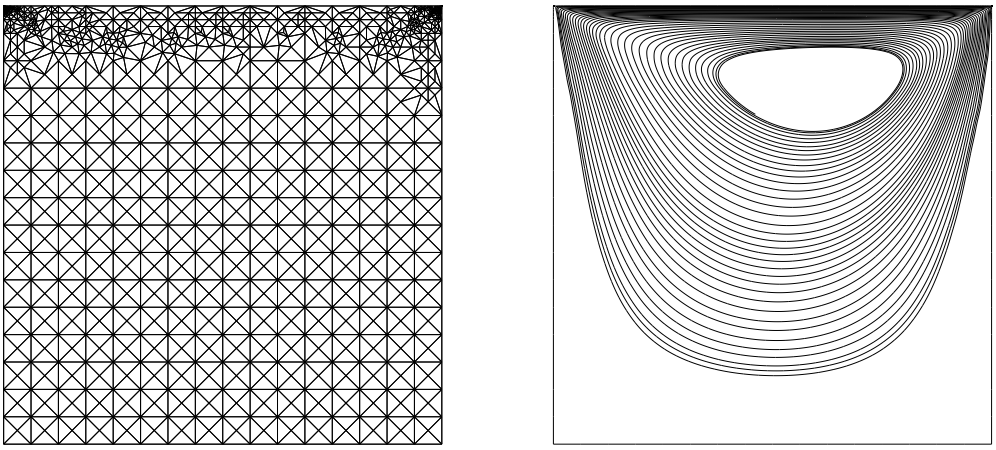

Fig. 8. Lid–Driven Cavity problem for $\nu = 10^{-2}$ and $\sigma = 1$. Adaptive mesh and streamlines. The number of nodes of the mesh is 1.255 nodes.

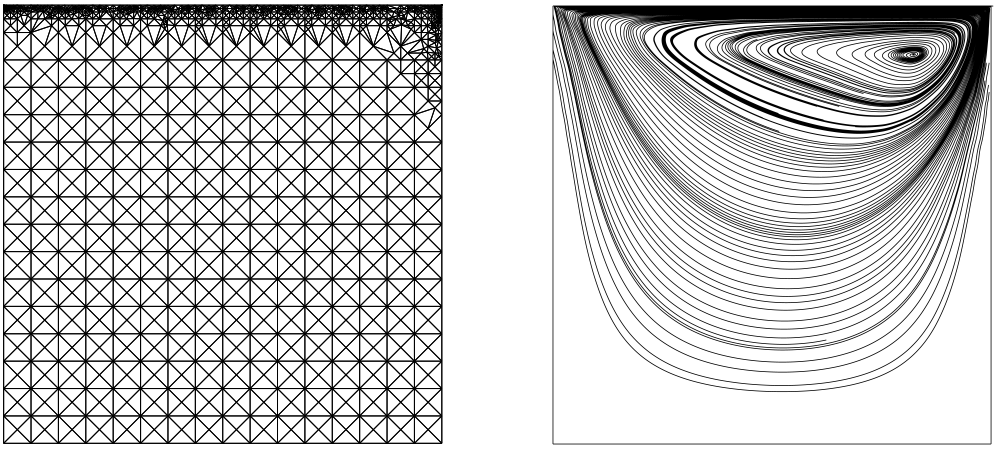

Fig. 9. Lid–Driven Cavity problem for $\nu = 10^{-3}$ and $\sigma = 1$. Adaptive mesh and streamlines. The number of nodes of the mesh is 1.626 nodes.

Figure 10 depicts the adaptive process that has taken place for the $\nu = 1/5000$ case. The adapted meshes improves the quality of the numerical solution as the vertical profile of the tangential velocity field shows in Figure 11. Indeed, we note the boundary layer is utterly free of spurious of oscillations thanks to the combined adaptive strategy.

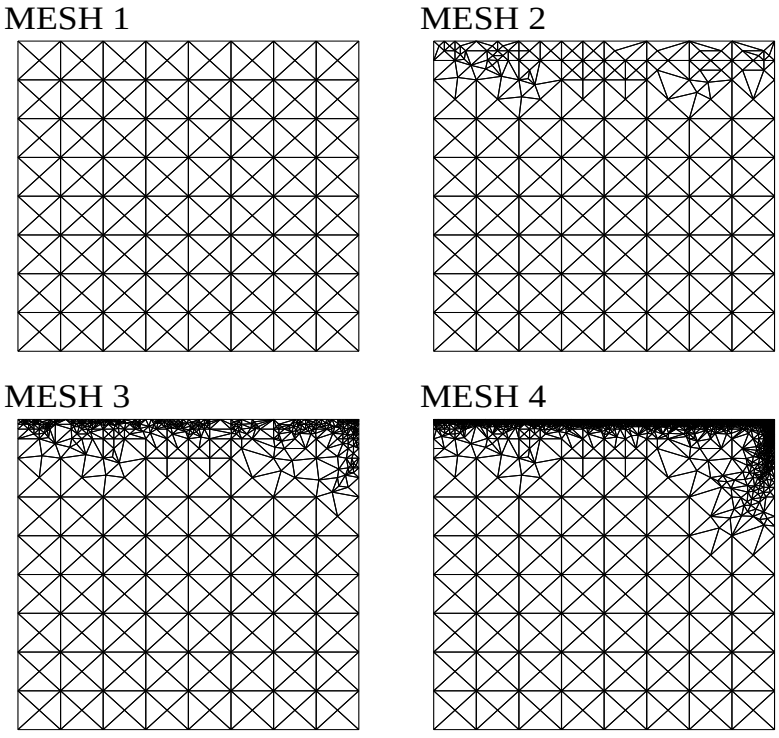

Fig. 10. Lid–Driven Cavity problem for $\nu = 1/5000$ and $\sigma = 1$. Sequence of adaptive meshes. The final mesh has 5.458 nodes.

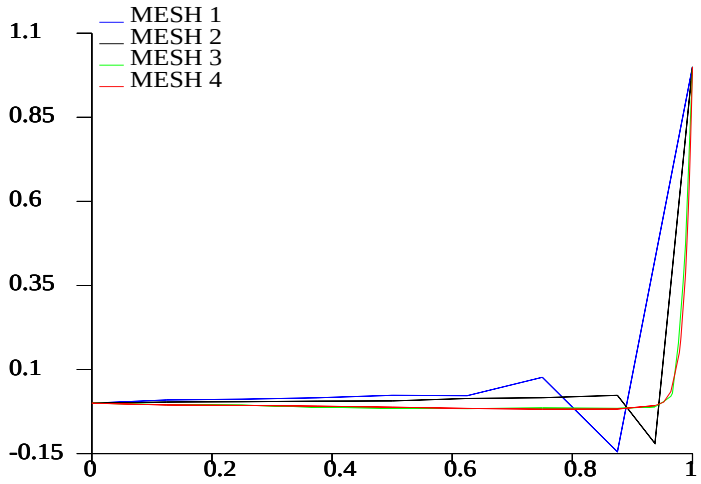

Fig. 11. Lid–Driven Cavity problem for $\nu = 1/5000$ and $\sigma = 1$. Tangential velocity profiles at $x = 0.5$ using the sequence of adaptive meshes.

5.3 Flow over a circular cylinder

The domain geometry and the boundary conditions are shown in Figure 12. The inflow velocity field is given by $\boldsymbol{u}_p = (1.2\, y\, (0.41 - y)/0.41^2, 0)^T$ (see [41] for further details).

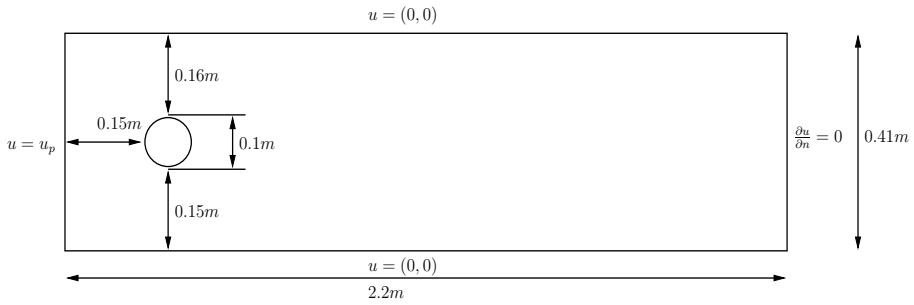

Fig. 12. Boundary conditions for the problem.

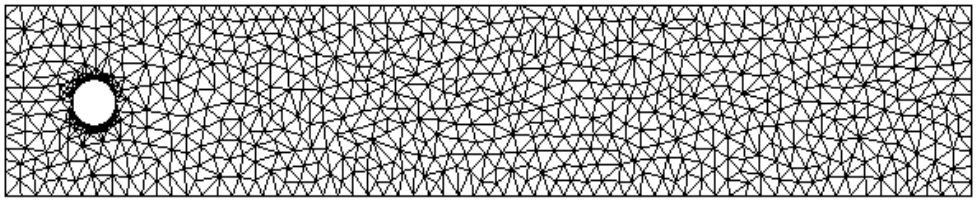

Fig. 13. Flow over a circular cylinder. The initial mesh.

5.3.1 First case: $\sigma = 0$

In this case we set $\nu = 10^{-3}$, and so, we expect meshes to be locally refined around the cylinder as a boundary layer is presented there. In Figure 14 a zoom of the initial and final adapted meshes around the cylinder are depicted. Isovalues of the magnitud of the velocity and the pressure indicate that numerical solutions are qualitatively improved (see Figures 15 and 16).

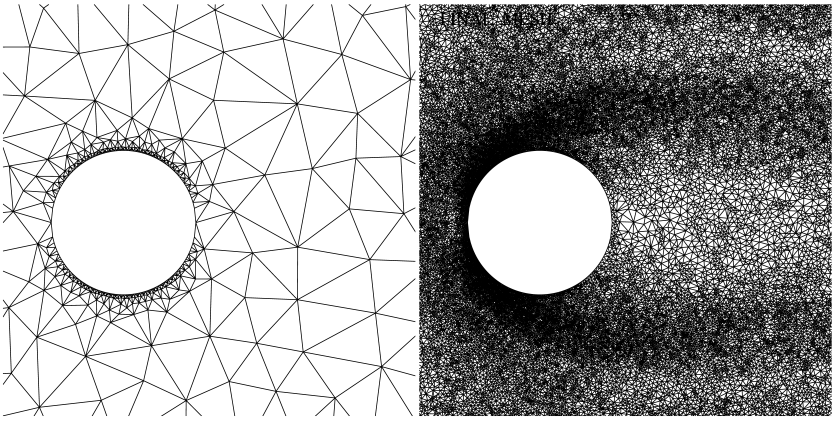

Fig. 14. Flow over a circular cylinder. A zoom around the cylinder showing the initial (left) and the final (right) meshes.

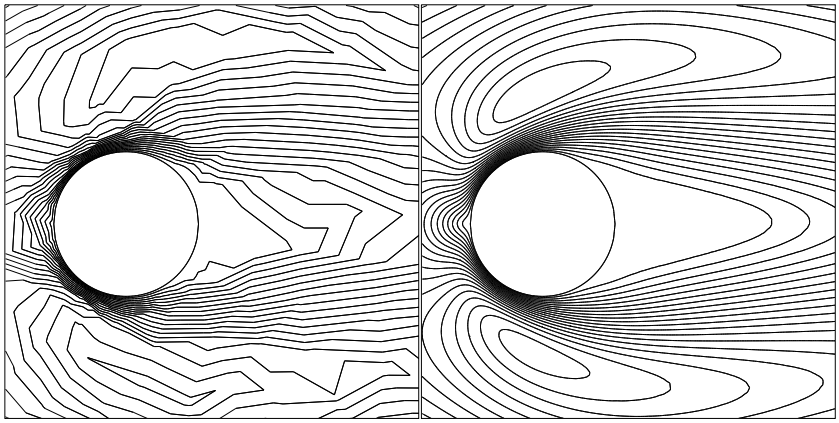

Fig. 15. Flow over a circular cylinder. Isolines of $|\boldsymbol{u}|$ from initial (left) and final (right) meshes.

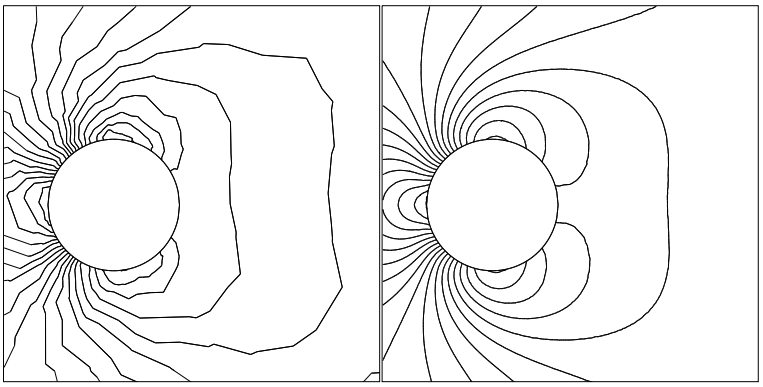

Fig. 16. Flow over a circular cylinder. Isolines of the pressure from the initial (left) and final (right) meshes.

5.3.2 Second case: $\sigma = 1$

.

Now, we validate a reactive flow using $\nu = 1$, $\nu = 10^{-3}$, $\nu = 10^{-5}$. It is worth pointing that the solutions of the latter case must be considered in average terms once the real flow is turbulent. Stabilized methods used for turbulence flow modeling is currently theme of researches (see for instance [9]).

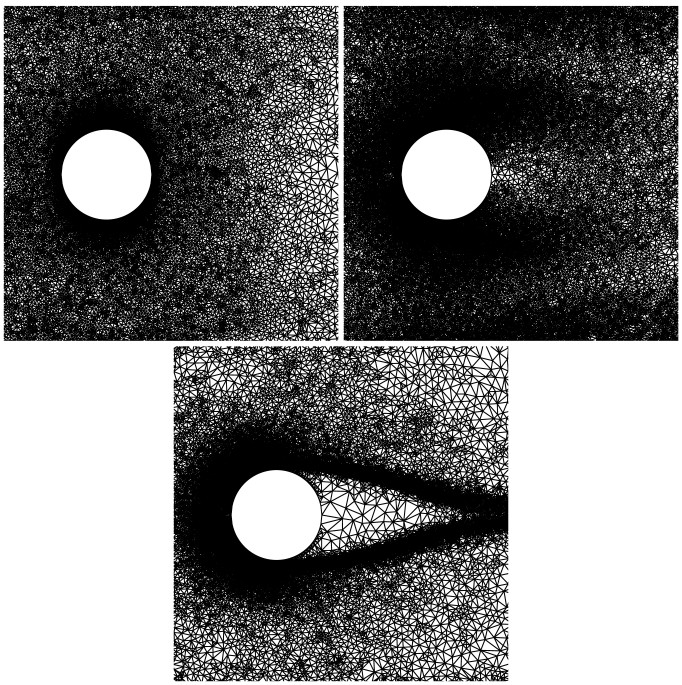

Fig. 17. Flow over a circular cylinder. Zoom of the adaptive mesh using $\sigma = 1$ and $\nu = 1$ (left top), $\nu = 10^{-3}$ (left top) and $\nu = 10^{-5}$ (bottom).

Figure 17 presents a zoom around the cylinder for the different values of ν. The increased influence of the coefficient σ on the solutions as ν goes to zero is noted. To show how well the adapted process improves the quality of the approximate solution, the Figure 18 presents a zoom of the isovalues of the $|\boldsymbol{u}|$ in the three cases. In addition, Figure 19 depicts the fully final adapted mesh for the whole domain for the case $\nu = 10^{-5}$. The mesh is accuretly refined near the cylinder and at the top and at the bottom of the domain. Finally, Figures 20 and 21 present the isolines of $|\boldsymbol{u}|$ and the pressure in the whole domain.

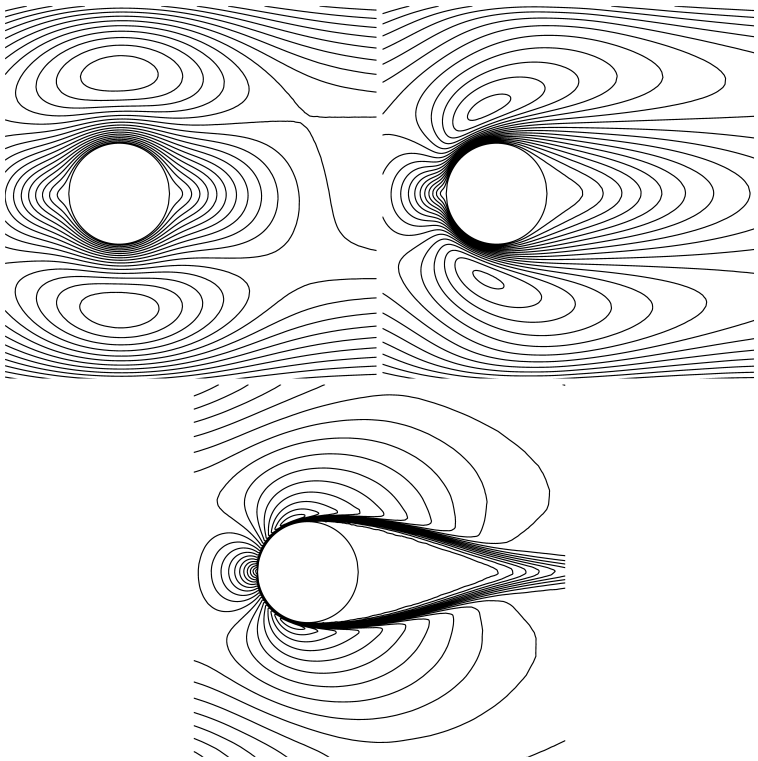

Fig. 18. Flow over a circular cylinder. Zoom of the isovalues $|\boldsymbol{u}|$ using $\sigma = 1$ and $\nu = 1$ (left top), $\nu = 10^{-3}$ (righ top) and $\nu = 10^{-5}$ (bottom).

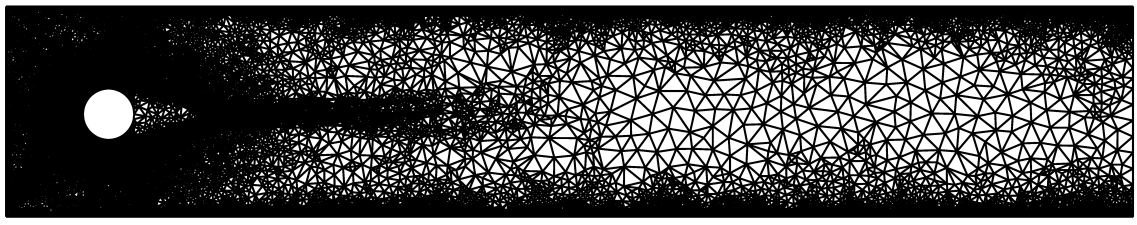

Fig. 19. Flow over a circular cylinder with $\nu = 10^{-5}$ and $\sigma = 1$. The final adaptive mesh. The number of nodes of the mesh is 84.409.

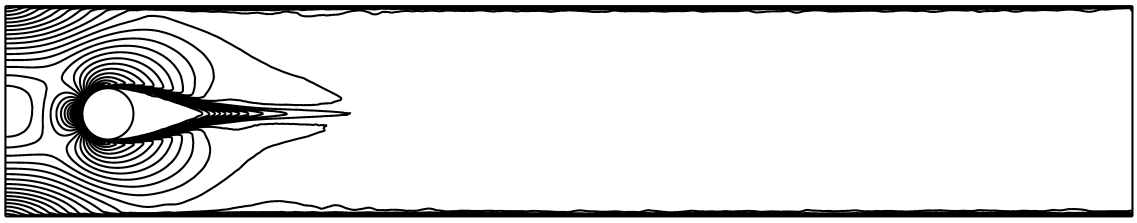

Fig. 20. Flow over a circular cylinder with $\nu = 10^{-5}$ and $\sigma = 1$. Isolines of $|\boldsymbol{u}|$.

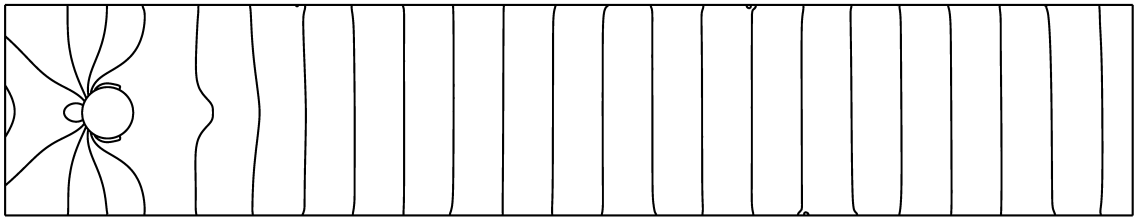

Fig. 21. Flow over a circular cylinder with $\nu = 10^{-5}$ and $\sigma = 1$. Isolines of the pressure.

Acknowledgements

This work was partially supported by CONICYT through FONDECYT Projects 1070698, 7080170, FONDAP and BASAL projects CMM, Universidad de Chile and CI2MA, Universidad de Concepción, CONICYT Fellowship and by CNPq/Brazil grant No. 304051/2006-3, FAPERJ/Brazil grant No. E-26/100.519/2007 and CAPES/Brazil.

References

[1] M. Ainsworth and J. T. Oden. *A posteriori error estimation in finite element analysis*. Pure and Applied Mathematics (New York). John Wiley & Sons, New York, 2000.

[2] R. Almeida and A. C. Galeão. An adaptive Petrov-Galerkin formulation for the compressible Euler and Navier–Stokes equations. *Comput. Methods Appl. Mech. Engrg.*, 129(1-2):157–176, 1996.

[3] R. Araya, G.R. Barrenechea, L. P. Franca, and F. Valentin. Stabilization arising from PGEM: A review and further developments. *Appl. Num. Math.* To appear.

[4] R. Araya, G.R. Barrenechea, and A. Poza. An adaptive stabilized finite element method for the generalized Stokes problem. *J. Comput. Appl. Math.*, 214(2):457–479, 2008.

[5] R. Araya and F. Valentin. A multiscale a posteriori error estimate. *Comput. Methods Appl. Mech. Engrg.*, 194:2077–2094, 2005.

[6] W. Bangerth and R. Rannacher. *Adaptive finite element methods for differential equations.* Lectures in Mathematics ETH Zürich. Birkhäuser Verlag, Basel, 2003.

[7] G.R. Barrenechea and F. Valentin. An unusual stabilized finite element method for a generalized Stokes problem. *Numer. Math.*, 92(4):653–677, 2002.

[8] G.R. Barrenechea and F. Valentin. Relationship between multiscale enrichment and stabilized finite element methods for the generalized Stokes problem. *CRAS*, 341(10):635–640, 2005.

[9] Y. Bazilevs, V. M. Calo, J. A. Cottrell, T. J. R Hughes, A. Reali, and G. Scovazzi. Variational multiscale residual-based turbulence modeling for large eddy simulation of incompressible flows. *Comput. Methods Appl. Mech. Engrg.*, 197(1-4):173–201, 2007.

[10] R. Becker. An optimal-control approach to a posteriori error estimation for finite element discretizations of the Navier–Stokes equations. *East-West J. Numer. Math.*, 8(4):257–274, 2000.

[11] R. Becker and R. Rannacher. A general concept of adaptivity in finite element methods with applications to problems in fluid and structural mechanics. In *Grid generation and adaptive algorithms (Minneapolis, MN, 1997)*, volume 113 of *IMA Vol. Math. Appl.*, pages 51–75. Springer, New York, 1999.

[12] S. Berrone. Adaptive discretization of stationary and incompressible Navier–Stokes equations by stabilized finite element methods. *Comput. Methods Appl. Mech. Engrg.*, 190(34):4435–4455, 2001.

[13] F. Brezzi and M. Fortin. *Mixed and hybrid finite element methods.* Springer-Verlag, New York, 1991.

[14] E. Burman, M. A. Fernández, and P. Hansbo. Continuous interior penalty finite element method for Oseen's equations. *Siam J. Numer. Anal.*, 44(3):1248–1274, 2006.

[15] Ph. Clément. Approximation by finite element functions using local regularization. *R.A.I.R.O. Anal. Numer.*, 9:77–84, 1975.

[16] R. Codina and O. Soto. Finite element solution of the Stokes problem with dominating Coriolis force. *Comput. Methods Appl. Mech. Engrg.*, 142(3-4):215–234, 1997.

[17] A. Ern and J.-L. Guermond. *Theory and practice of finite elements*, volume 159 of *Applied Mathematical Sciences*. Springer-Verlag, New York, 2004.

[18] L. P. Franca and S. Frey. Stabilized finite element methods: II. The incompressible Navier–Stokes equations. *Comput. Methods Appl. Mech. Engrg.*, 99:209–233, 1992.

[19] L.P. Franca and C. Farhat. Bubble functions prompt unusual stabilized finite element methods. *Comput. Methods Appl. Mech. Engrg.*, 123(1-4):299–308, 1995.

[20] L.P. Franca and A.L. Madureira. Element diameter free stability parameters for stabilized methods applied to fluids. *Comput. Methods Appl. Mech. Engrg.*, 105(3):395–403, 1993.

[21] L.P. Franca, A.L. Madureira, L. Tobiska, and F. Valentin. Convergence analysis of a multiscale finite element method for singularly perturbed problems. *SIAM Multiscale Model. and Simul.*, 4(3):839–866, 2005.

[22] L.P. Franca, A.L. Madureira, and F. Valentin. Towards multiscale functions: enriching finite element spaces with local but not bubble–like functions. *Comput. Methods Appl. Mech. Engrg.*, 194:3006–3021, 2005.

[23] L.P. Franca and P.S. Oliveira. Pressure bubbles stabilization features in the Stokes problem. *Comput. Methods Appl. Mech. Engrg.*, 192(16-18):1929–1937, 2003.

[24] L.P. Franca and A. Russo. Recovering SUPG using Petrov-Galerkin formulations enriched with adjoint Residual-Free Bubbles. *Comput. Methods Appl. Mech. Engrg.*, 182(3-4):333–339, 2000.

[25] L.P. Franca and R. Stenberg. Error analysis of Galerkin least squares methods for the elasticity equations. *SIAM J. Numer. Anal.*, 28(6):1680–1697, 1991.

[26] L.P. Franca and F. Valentin. On an improved unusual stabilized finite element method for the advective–reactive–diffusive equation. *Comput. Methods Appl. Mech. Engrg.*, 190(13–14):1785–1800, 2000.

[27] U. Ghia, K.N. Ghia, and C.T. Shin. High-Re solutions for incompressible flow using the Navier–Stokes equations and a multigrid method. *J. Comput. Phys*, 48(3):387–411, 1982.

[28] V. Girault and P.A. Raviart. *Finite element methods for the Navier–Stokes equations*. Springer-Verlag, Berlin, 1986.

[29] M.D. Gunzburger and J. S. Peterson. Predictor and steplength selection in continuation methods for the Navier–Stokes equations. *Comput. math. appl*, 22:73–81, 1991.

[30] I. Harari and T.J.R. Hughes. Stabilized finite element methods for steady advection–diffusion with production. *Comput. Methods Appl. Mech. Engrg.*, 115(1-2):165–191, 1994.

[31] G. Hauke. A simple subgrid scale stabilized finite element method for the advection–diffusion–reaction equation. *Comput. Methods Appl. Mech. Engrg.*, 191:2925–2947, 2002.

[32] T.J.R. Hughes, M. Mallet, and A. Mizukami. A new finite element formulation for computational fluid dynamics. II. Beyond SUPG. *Computer Methods in Applied Mechanics and Engineering*, 54(3):341–355, 1986.

[33] H. Jin and S. Prudhomme. A posteriori error estimation of steady-state finite element solutions of the Navier–Stokes equations by a subdomain residual method. *Comput. Methods Appl. Mech. Engrg.*, 159(1-2):19–48, 1998.

[34] Volker John. Residual a posteriori error estimates for two-level finite element methods for the Navier–Stokes equations. *Appl. Numer. Math.*, 37(4):503–518, 2001.

[35] C. T. Kelley. *Iterative methods for linear and nonlinear equations*, volume 16 of *Frontiers in Applied Mathematics*. Society for Industrial and Applied Mathematics (SIAM), Philadelphia, PA, 1995.

[36] T. J. Oden, W. Wu, and M. Ainsworth. An a posteriori error estimate for finite element approximations of the Navier–Stokes equations. *Comput. Methods Appl. Mech. Engrg.*, 111(1-2):185–202, 1994.

[37] R. Renka. Algorithm 660: QSHEP2D, Quadratic Shepard method for bivariate interpolation of scattered data. *ACM Trans. Math. Softw.*, 14:149–150, 1988.

[38] H. Roos, M. Stynes, and L. Tobiska. *Numerical methods for singularly pertubed differential equations*. Springer, 1991.

[39] J. R. Shewchuk. Triangle: Engineering a 2D Quality Mesh Generator and Delaunay Triangulator. In *Applied Computational Geometry: Towards Geometric Engineering*, volume 1148 of *Lecture Notes in Computer Science*, pages 203–222. Springer-Verlag, 1996.

[40] L. Tobiska and R. Verfürth. Analysis of a Streamline Diffusion Finite Element Method for the Stokes and Navier–Stokes Equations. *SIAM J. Numer. Anal.*, 33:107–127, 1996.

[41] S. Turek. *Efficient solvers for incompressible flow problems*, volume 6 of *Lecture Notes in Computational Science and Engineering*. Springer-Verlag, Berlin, 1999.

[42] R. Verfürth. *A review of a posteriori error estimation and adaptative mesh refinement techniques*. Wiley–Teubner, 1996.